OPEN ACCESS
CellPress

Cell Reports
Article

APP Homodimers Transduce an Amyloid-β-Mediated Increase in Release Probability at Excitatory Synapses

Hilla Fogel,[1,7] Samuel Frere,[1,7] Oshik Segev,[1] Shashank Bharill,[4] Ilana Shapira,[1] Neta Gazit,[1,2] Tiernan O'Malley,[5,6] Edden Slomowitz,[1] Yevgeny Berdichevsky,[1] Dominic M. Walsh,[6] Ehud Y. Isacoff,[4] Joel A. Hirsch,[3] and Inna Slutsky[1,2,*]
[1]Department of Physiology and Pharmacology, Sackler Faculty of Medicine, Tel Aviv University, 69978 Tel Aviv, Israel
[2]Sagol School of Neuroscience, Tel Aviv University, 69978 Tel Aviv, Israel
[3]Department of Biochemistry and Molecular Biology, George S. Wise Faculty of Life Sciences, Tel Aviv University, 69978 Tel Aviv, Israel
[4]Department of Molecular and Cell Biology and Helen Wills Neuroscience Institute, University of California Berkeley, Berkeley, CA 94720, USA
[5]Laboratory for Neurodegenerative Research, School of Biomolecular and Biomedical Science, Conway Institute, University College Dublin, Dublin 4, Republic of Ireland
[6]Laboratory for Neurodegenerative Research, Center for Neurologic Diseases, Brigham & Women's Hospital, Harvard Institutes of Medicine, Boston, MA 02115, USA
[7]Co-first author
*Correspondence: islutsky@post.tau.ac.il
http://dx.doi.org/10.1016/j.celrep.2014.04.024

SUMMARY

Accumulation of amyloid-β peptides (Aβ), the proteolytic products of the amyloid precursor protein (APP), induces a variety of synaptic dysfunctions ranging from hyperactivity to depression that are thought to cause cognitive decline in Alzheimer's disease. While depression of synaptic transmission has been extensively studied, the mechanisms underlying synaptic hyperactivity remain unknown. Here, we show that Aβ40 monomers and dimers augment release probability through local fine-tuning of APP-APP interactions at excitatory hippocampal boutons. Aβ40 binds to the APP, increases the APP homodimer fraction at the plasma membrane, and promotes APP-APP interactions. The APP activation induces structural rearrangements in the APP/$G_{i/o}$-protein complex, boosting presynaptic calcium flux and vesicle release. The APP growth-factor-like domain (GFLD) mediates APP-APP conformational changes and presynaptic enhancement. Thus, the APP homodimer constitutes a presynaptic receptor that transduces signal from Aβ40 to glutamate release. Excessive APP activation may initiate a positive feedback loop, contributing to hippocampal hyperactivity in Alzheimer's disease.

INTRODUCTION

Accumulation of amyloid-β (Aβ) in the extracellular space of the brain appears to be critical for developing synaptic and cognitive deficits in Alzheimer's disease (AD) (Palop and Mucke, 2010). Aβ is produced by sequential limited proteolysis of the amyloid precursor protein (APP), a type I single-transmembrane-span protein (Kang et al., 1987), by two aspartyl proteases, β- and γ-secretases. Normally, γ-secretase cleavage results in variable 38- to 43-amino-acid Aβ peptides, with Aβ40 monomers as the predominant species. The biophysical and biochemical properties of Aβ strongly depend on its concentration, length, and primary structure. Gradual elevation of Aβ monomers in limbic and association cortices leads to its aggregation into oligomers, prefibrillar assemblies (protofibrils), and amyloid fibrils. All of these Aβ forms may be in dynamic equilibrium, leading to a high variety of synaptic and circuit dysfunctions that underlie progressive cognitive impairments in AD (Mucke and Selkoe, 2012). Transient upregulation of Aβ production or application of pathological Aβ levels depresses excitatory synaptic transmission (Hsia et al., 1999; Kamenetz et al., 2003). Soluble Aβ oligomers have been suggested to cause postsynaptic depression of glutamatergic transmission via loss of dendritic spines, blockade of long-term potentiation, and increase in long-term synaptic depression (Shankar et al., 2008; Walsh et al., 2002).

While pathological Aβ concentrations and assembly forms depress excitatory synaptic function through postsynaptic mechanisms, an increase in endogenous Aβ levels induced by inhibition of extracellular Aβ degradation causes presynaptic enhancement (Abramov et al., 2009). Specifically, inhibition of the Aβ-degrading enzyme neprilysin augmented glutamate release probability, reduced short-term facilitation of excitatory synaptic currents, and increased excitation-inhibition balance in hippocampal circuits (Abramov et al., 2009). Because hippocampal and cortical hyperactivity is common in various transgenic AD mouse models (Busche et al., 2008, 2012; Palop et al., 2007; Verret et al., 2012), in humans with mild cognitive impairments (Bakker et al., 2012), and in AD patients (Vossel et al., 2013), elucidating the synaptic mechanisms of hyperactivity is critical for understanding AD-associated cognitive impairments.

In the current study, we explored the mechanism initiating augmentation of synaptic vesicle release at excitatory

hippocampal synapses by increasing the extracellular Aβ concentration ($[A\beta]_o$) in cultured hippocampal neurons and acute hippocampal slices. Utilizing a combination of fluorescence resonance energy transfer (FRET) spectroscopy, a single-molecule imaging, two-photon excitation laser scanning microscopy combined with fluorescence lifetime imaging (2pFLIM), biochemistry, and imaging of synaptic vesicle recycling and of calcium, we found that the APP homodimer constitutes a presynaptic Aβ40 receptor mediating the regulation of release probability at excitatory hippocampal synapses.

RESULTS

APP Is Essential for Aβ-Mediated Presynaptic Enhancement

Concentrations of Aβ in the synaptic cleft are determined by the balance of Aβ production, release, and degradation. We have previously shown that inhibition of neprilysin, an Aβ-degrading enzyme, increases release probability in excitatory hippocampal synapses (Abramov et al., 2009). Inhibition of neprilysin was ineffective in $APP^{-/-}$ neurons, suggesting that APP and/or Aβ mediate the presynaptic enhancement. Here, we wished to determine whether APP, in addition to being the source for Aβ, is also necessary for Aβ-induced signaling leading to the augmentation of basal transmitter release. We examined the effect of human $A\beta_{1-40}$ (Aβ40), the most abundant Aβ isoform, on basal synaptic vesicle recycling in cultured hippocampal neurons using the activity-dependent dye FM1-43 as described earlier (Abramov et al., 2009). To this end, we quantified the total amount of releasable fluorescence at each bouton (ΔF) and the density of FM^+ puncta per image (D) following stimulation (30 action potentials at a rate of 0.2 Hz; Figure S1A) in the presence of 10 μM FM1-43. Figure 1A illustrates a typical high-magnification ΔF image before and after Aβ40 application. The total presynaptic strength within a given region of the hippocampal network (S) can be estimated as the product of ΔF and D ($S = \Delta F \times D$). First, we measured the effect of size-exclusion chromatography-isolated Aβ40 monomers (Figure S2) on synaptic vesicle turnover in cultured hippocampal neurons from wild-type (WT) mice. Our results demonstrate that acute application of Aβ40 monomers (100 pM, 15 min) induced a substantial increase in both ΔF and D across synaptic populations, resulting in a 2-fold increase in the total presynaptic strength S in WT neurons (Figures 1B and 1C). The collective results of these experiments show a profound increase of S by Aβ40 monomers in a concentration-dependent manner (Figure 1I). Application of rat Aβ40 monomers produced a similar effect on presynaptic strength (data not shown). Because covalently crosslinked Aβ40 dimers ($[A\beta40S26C]_2$) have been shown to enhance Ca^{2+} transients in CA1 hippocampal neurons in vivo (Busche et al., 2012), we assessed their effects (O'Nuallain et al., 2010; Figure S2) on presynaptic function. Notably, fresh $[A\beta40S26C]_2$ produced a presynaptic enhancement (100 pM; Figure 1D) similar to the one induced by 100 pM Aβ40 monomers.

Next, we assessed the effect of Aβ40 in hippocampal neurons produced from $APP^{-/-}$ (Zheng et al., 1995) mice. Surprisingly, the same concentrations of Aβ40 monomers or Aβ40S26C dimers that increased presynaptic activity in WT neurons were ineffective in neurons lacking APP (Figures 1E–1I). Expression of WT APP in $APP^{-/-}$ neurons rescued the presynaptic effect of Aβ40 (Figure S1B), suggesting that both Aβ40 and its precursor, APP, are essential for augmentation of synaptic vesicle recycling. Notably, the presynaptic Aβ40 effect was not altered by several Aβ binding candidates such as cellular prion protein (PrP^C) or α7 nicotinic acetylcholine receptor (α7nAChR), because Aβ40 was still able to potentiate synaptic vesicle recycling in hippocampal neurons produced from PrP^C knockout mice or following blockade of α7nAChR by α-bungarotoxin (Figure S1B). Taken together, these results suggest that APP is necessary for the presynaptic signaling mediated by Aβ40 monomers and dimers.

Monitoring APP-APP Interactions at Individual Hippocampal Boutons

Previous studies in heterologous expression systems suggest that APP molecules can form homodimers and that APP homodimerization may regulate Aβ production (Eggert et al., 2009; Munter et al., 2007). Having established a critical role of APP in the Aβ40-mediated presynaptic enhancement, we next explored the relationship between APP-APP interactions and synapse release probability at individual hippocampal synapses. First, we tested whether APP forms homodimers at the presynaptic compartments. FRET spectroscopy enables studying conformational changes between fluorescently tagged proteins at the single-synapse level (Laviv et al., 2010) by providing an accurate measure of possible changes in the relative distance (<100 Å) and/or orientation between fluorophores. We transfected hippocampal cultures with APP C-terminally tagged with mCitrine (APP^{Cit}) and with Cerulean (APP^{Cer}) (Figure 2A). FRET measurements were taken from boutons of hippocampal neurons (Figures 2B and S4A). Presynaptic localization of the tagged APP molecules in boutons was confirmed by colocalization of APP^{Cit} with cyan fluorescent protein (CFP)-tagged synapsin Ia protein (data not shown). We measured the steady-state mean FRET efficiency (E_m) utilizing the acceptor photobleaching method (Figures 2C and 2D), which dequenches the donor (Cer). FRET efficiency was measured in the presence of tetrodotoxin (TTX), which blocks spike generation, allowing only miniature synaptic release. To estimate E_m using a spectroscopic approach, Cer/Cit emissions were collected in the range of 400–600 nm using a 440 nm excitation wavelength at individual presynaptic boutons expressing APP^{Cer} and APP^{Cit} proteins. A typical emission spectrum is displayed in Figure 2D. High-magnification confocal images (Figure 2B) of the presynaptic bouton (marked by arrowhead) show an increase in Cer fluorescence after Cit photobleaching (Figure 2C), indicating dequenching of the donor and the presence of FRET. Quantitative analysis of FRET signals between APP^{Cer} and APP^{Cit} proteins across 86 functional boutons from seven experiments under miniature synaptic activity revealed a mean E_m of 0.14 ± 0.01 (Figure 2E). The FRET level varied across different boutons (coefficient of variation of 77%), suggesting different APP-APP conformational states at the single-bouton level. Notably, higher FRET levels were detected between APP^{Cer} and APP^{Cit} proteins expressed in $APP^{-/-}$ cultures, which were significantly reduced by coexpression of the nontagged APP (APP^{NT}, Figure 2E). These data

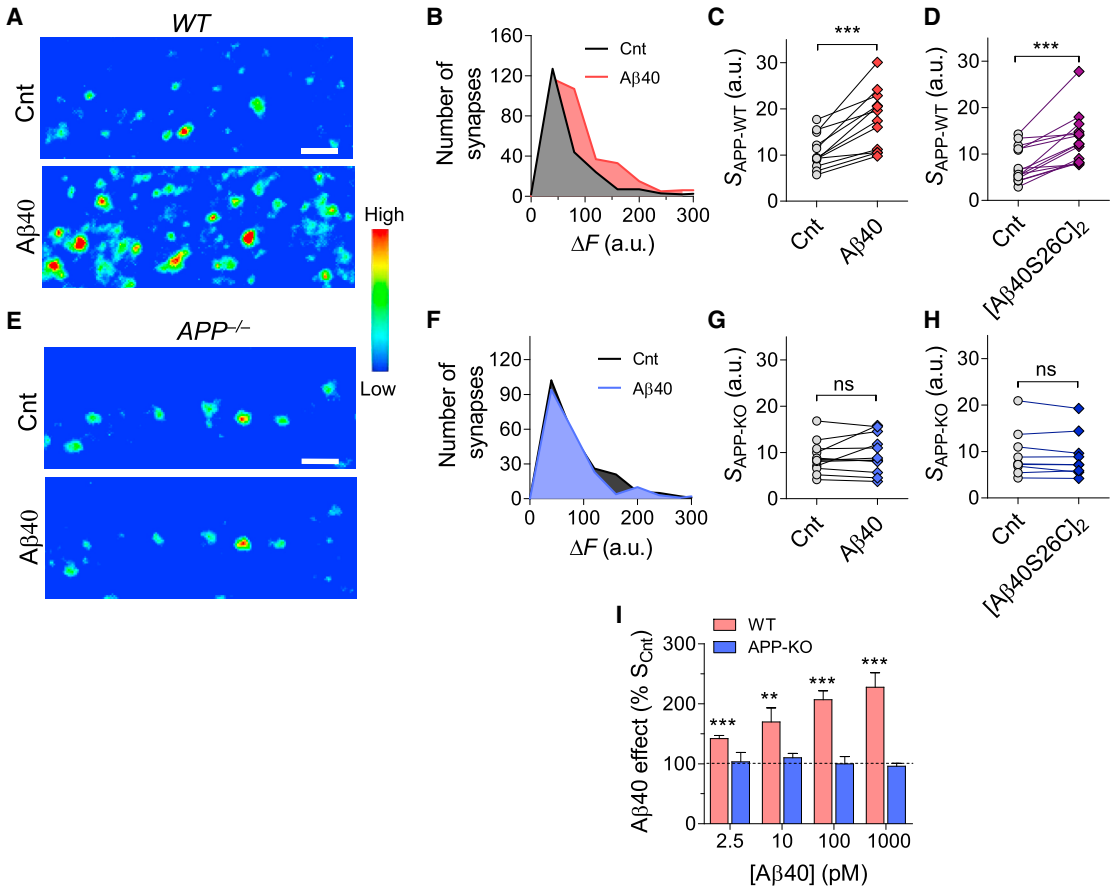

Figure 1. APP Is Required for Aβ40-Induced Presynaptic Enhancement

(A) Representative Δ*F* images before and 15 min after application of 100 pM Aβ40 monomers in WT hippocampal culture. Stimulation during FM1-43 staining: 30 action potentials at 0.2 Hz; destaining: 1,000 action potentials at 2 Hz. Fluorescence intensities (arbitrary units [a.u.]) are coded using a pseudo-color transformation. Scale bar, 2 μM.

(B) Δ*F* histograms before and after 100 pM Aβ40 monomers application in a single experiment in WT hippocampal culture. The mean *F* increased from 76 to 100 a.u., and the number of FM (+) puncta increased from 220 to 331.

(C) Effects of Aβ40 monomers (100 pM) on the total presynaptic strength in WT neurons ($S_{APP\text{-}WT}$, N = 12).

(D) Effects of Aβ40S26C dimers (100 pM) on the total presynaptic strength in WT neurons ($S_{APP\text{-}WT}$, N = 14).

(E) Representative Δ*F* images before and 15 min after application of Aβ40 monomers in $APP^{-/-}$ neurons. Stimulation during FM1-43 staining: 30 action potentials at 0.2 Hz; destaining: 1,000 action potentials at 2 Hz. Scale bar, 2 μM.

(F) Δ*F* histograms before and after 100 pM Aβ40 monomers application in a single experiment in $APP^{-/-}$ neurons.

(G) Aβ40 monomers (100 pM) do not affect the total presynaptic strength in $APP^{-/-}$ neurons ($S_{APP\text{-}KO}$, N = 12).

(H) $[Aβ40S26C]_2$ (100 pM) do not affect the total presynaptic strength in $APP^{-/-}$ neurons ($S_{APP\text{-}KO}$, N = 9).

(I) Aβ40 monomers increase S in a dose-dependent manner in WT (N = 7–12), but not in $APP^{-/-}$ (N = 6 – 12, $p > 0.3$), neurons. Error bars represent SEM.

indicate that either endogenous or exogenous nontagged APP molecules interact with the tagged APP, resulting in FRET reduction as predicted. Quantification of APP^{Cit} expression in axons of $APP^{-/-}$ neurons demonstrated amounts lower than or comparable to endogenous presynaptic APP expression in WT neurons (Figure S3), suggesting that FRET can occur under physiologically relevant APP levels. To rule out nonspecific association due to overexpression of the tagged proteins, we cotransfected APP^{Cer} and a nonrelated protein subunit of $GABA_BRs$, GB_{1a}, C-terminally tagged with Cit ($GB_{1a}{}^{Cit}$). These two tagged proteins showed negligible FRET (Figure 2E). Furthermore, background enhancement of Cer emission, assessed by photobleaching at 515 nm in neurons expressing only APP^{Cer}, was <2% (Figure 2E). Therefore, the higher FRET efficiencies measured between APP^{Cer} and APP^{Cit} ($p < 0.0001$) are due to the specific associations of APP^{Cer} and APP^{Cit} proteins. Altogether, these data indicate that individual APP molecules occur in close proximity in excitatory hippocampal boutons.

APP-APP Interactions Correlate to Release Probability at Excitatory Synapses

Because release probability is highly heterogeneous across hippocampal synapses (Laviv et al., 2010), we asked whether APP-APP interactions vary across individual synapses and correlate to synapse release probability. To directly address these questions, we monitored FM destaining kinetics, a reliable

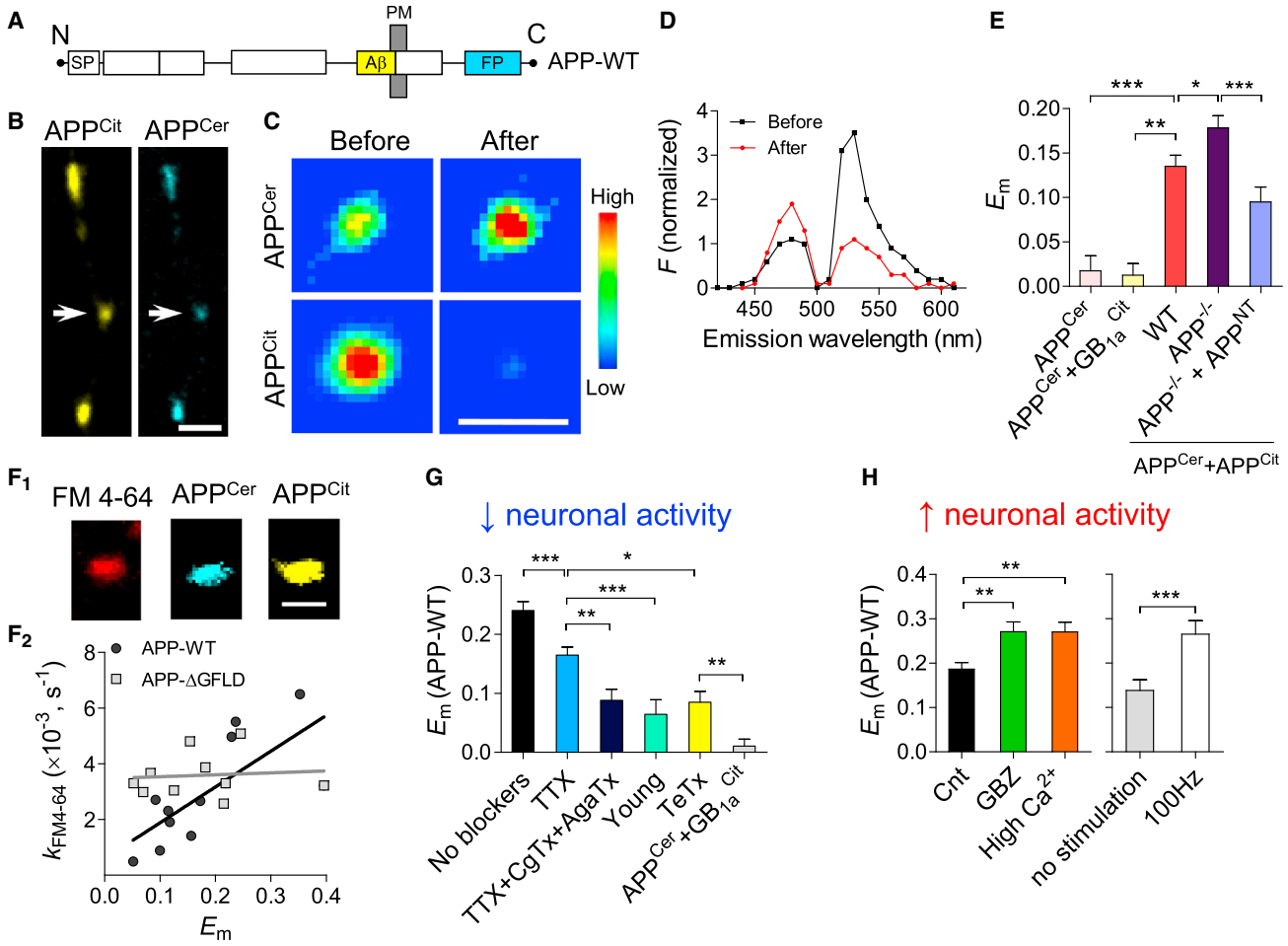

Figure 2. APP Molecules form Homodimers in Activity-Dependent Manner at Single Hippocampal Boutons

(A) Schematic illustration of the fusion protein construct between APP and fluorophore (FP) used for FRET detection.

(B) Representative confocal images of hippocampal boutons of pyramidal neuron shown in Figure S4A that was cotransfected with APP^{Cit} and APP^{Cer}. Arrowheads show the bouton that was bleached for calculation of FRET efficiency in (C). Scale bar, 2 μm.

(C) Pseudo-color-coded fluorescent images of APP^{Cit} and APP^{Cer} proteins expressed in a hippocampal bouton before and after Cit photobleaching. Note the increase of Cer fluorescence (ex: 440 nm; em: 470–500 nm) after Cit (ex: 515 nm; em: 530–560 nm) photobleaching. Scale bar, 1 μM.

(D) Detection of mean FRET efficiency (E_m) by spectral approach under 440 nm excitation in a single bouton. The donor emission peak is shown before and after photobleaching.

(E) Summary of E_m data for APP^{Cer} only (n = 13), APP^{Cer} /$GB1a^{Cit}$ (n = 21), APP^{Cer}/APP^{Cit} expressed in WT neurons (n = 86), APP^{Cer}/APP^{Cit} expressed in $APP^{-/-}$ neurons (n = 38) and APP^{Cer}/APP^{Cit} expressed in $APP^{-/-}$ neurons with nontagged APP (APP-NT: n = 22). Error bars represent SEM.

(F) Measurement of release probability using FM4-64 and E_m between APP^{Cer} and APP^{Cit} at the single-bouton level (F_1). Scale bar, 1 μM. (F_2) Pooled data across 12 boutons reveal a positive correlation between E_m and the FM4-64 decay rate constant (Spearman r = 0.8, $p < 0.01$) but no correlation between the APP-$\Delta GFLD^{Cer}$-APP-$\Delta GFLD^{Cit}$ homodimer and the FM4-64 decay rate constant (Spearman r = 0.2, $p > 0.6$).

(G) Reduction in neuronal and synaptic activity decreased APP^{Cer}-APP^{Cit} FRET efficiency: tetrodotoxin (TTX, 0.5 μM; n = 51–75, $p < 0.0001$); ω-conotoxin (CgTx) and ω-agatoxin (AgaTx) in the presence of TTX (n = 51–59, $p < 0.001$). E_m was decreased in immature neurons (4–5 DIV, young: n = 30, N = 6, $p < 0.01$) and by tetanus toxin (TeTx: n = 35, $p < 0.05$) and was significantly higher ($p < 0.01$) than nonspecific APP^{Cer}-$GB1a^{Cit}$ FRET. Error bars represent SEM.

(H) Increase in neuronal and synaptic activity induces an augmentation in APP^{Cer}-APP^{Cit} E_m: gabazine (GBZ: n = 40, N = 5, $p < 0.002$), an increase in $[Ca^{2+}]_o$ to 4.8 mM (High Ca^{2+}: n = 38, $p < 0.002$); high-frequency 100 Hz stimulation (n = 14, $p < 0.001$). The extracellular solution included AP-5 (50 μM) and DNQX (10 μM). Error bars represent SEM.

indicator of release probability, together with FRET efficiency measurements between APP^{Cer} and APP^{Cit} proteins at individual boutons of pyramidal hippocampal neurons. The total pool of recycling vesicles was stained by 600 action potentials at a rate of 10 Hz, and the colocalized FM4-64/Cer/Cit puncta were subjected to FRET analysis. The FM4-64 destaining rate (Figures S1C and S1D) and FRET efficiency between APP^{Cer} and APP^{Cit} subunits were measured during 1 Hz stimulation. The FM destaining rate constant ($k = 1/\tau_{decay}$, where τ_{decay} is an exponential time course) is proportional to the probability of vesicle release and was plotted against E_m between APP^{Cer} and APP^{Cit} for each imaged bouton (Figure 2F). The pooled data from 12

boutons demonstrate a positive correlation between E_m and the rate of FM destaining (Spearman r = 0.8, p < 0.01; Figure 2F$_2$). These results suggest that APP-APP interactions correlate to release probability in excitatory hippocampal boutons.

Regulation of APP-APP Interactions by Neuronal and Synaptic Activity

We next asked whether APP-APP interactions could be regulated by the level of neuronal and synaptic activity. Activity levels were altered using pharmacological agents or electrical stimulation. FRET efficiency under spontaneous neuronal activity was 0.24 ± 0.015 (no blockers, Figure 2G). Spike blockade by 0.5 μM TTX triggered a 33% decrease in E_m (p < 0.001; Figure 2G). To assess the changes in interactions between APP^{Cer} and APP^{Cit} in the same synapse before and after pharmacological treatment, we utilized the sensitized emission method by monitoring the ratio of Cit to Cer emission under Cer excitation (FRET ratio, defined as *FR*). *FR* was also lowered after TTX application (p < 0.0001; Figure S4A). Notably, TTX had no effect on E_m in APP molecules containing the endoplasmic reticulum (ER) retaining motif KKQN (Shaked et al., 2006) (APP-KK, p = 0.75; Figure S4B). Noteworthy, FRET between APP-KK was reduced, but not abolished, indicating that the pool of APP in the ER exists also as a complex. These results indicate that neuronal activity may alter the number and/or conformation of APP-APP complexes at the plasma membrane.

To test whether APP-APP interactions are regulated by neurotransmitter release, we measured the effects of presynaptic calcium channels or soluble NSF attachment protein receptor (SNARE)-dependent exocytosis blockers on APP conformation. Blocking presynaptic Ca^{2+} flux through N- and P/Q-type calcium channels by ω-conotoxin and ω-agatoxin resulted in reduction of E_m by 62% (p < 0.01; Figure 2G). Notably, measuring FRET between APP^{Cer} and APP^{Cit} in immature (3–4 days in vitro [DIV]) neurons, which lack the ability to recycle vesicles, revealed a 75% reduction in E_m (p < 0.01; Figure 2G) compared with mature (12–14 DIV) cultured neurons. Finally, blocking SNARE-dependent vesicle exocytosis by tetanus toxin (TeTx) reduced FRET by 65% (p < 0.05; Figure 2G) but did not completely abolish FRET between APP^{Cer} and APP^{Cit} as revealed by a comparison to the negative control (between APP^{Cer} and GB1a^{Cit}, p < 0.01; Figure 2G). These results indicate that synaptic activity is not necessary for the basal APP-APP precoupling but is required for the modulation of interactions between APP molecules.

Next, we explored whether these APP-APP interactions can be tuned by spiking and synaptic release properties in the opposite direction as well. Boosting neuronal activity by applying the GABA(A) receptor blocker gabazine (GBZ, 30 μM) or by elevating the extracellular Ca^{2+} levels from 1.2 to 4.8 mM (high Ca^{2+}) caused a 42% increase in FRET in both cases (p < 0.002; Figures 2H and S4C). Moreover, high-frequency (100 Hz) stimulation of neurons triggered an 86% increase in FRET (p < 0.0001; Figure 2H and S4D). Notably, high-frequency stimulation had no effect on E_m in the presence of TeTx (Figure S4E), indicating that SNARE-dependent vesicle release is required for changes in APP-APP interactions. Altogether, these results indicate that APP-APP interactions are positively modulated by neuronal and synaptic activity.

Aβ as the Mediator of Activity-Dependent APP-APP Interactions

Because extracellular Aβ concentration is directly regulated by neuronal and synaptic activity (Cirrito et al., 2005; Kamenetz et al., 2003), we asked whether Aβ employs feedback regulation by mediating the APP-APP conformational changes. To this end, we utilized APP-M596V, which contains a point mutation that blocks β-secretase cleavage and therefore Aβ production (Citron et al., 1995). APP-M596V^{Cer} and APP-M596V^{Cit} were transfected in APP-KO cultures to ensure the lack of Aβ production and release. APP-M596V resulted in 2-fold lower (p < 0.0001) basal FRET (0.12 ± 0.014; Figure 3A, no blockers) compared to APP-WT (Figure 2G, no blockers). Moreover, APP-M596V abolished bidirectional APP-APP FRET changes by neuronal activity (p > 0.6; Figure 3A).

We then directly explored the ability of Aβ to induce APP-APP conformational changes. First, we examined whether Aβ40 induces FRET changes between the tagged APP molecules in a heterologous expression system using human embryonic kidney 293 cells. Aβ40 induced a 28% increase in the APP-APP FRET ratio (p < 0.0001; Figures S5A and S5B). We next assessed the direct effects produced by changes in $[Aβ]_o$ on FRET between APP^{Cer} and APP^{Cit} expressed in presynaptic boutons of hippocampal neurons. Application of 100 pM Aβ40 monomers or AβS26C dimers to WT neurons increased E_m by 65% ± 12% and 58% ± 16%, respectively (Figure 3B). Aβ40 monomers triggered a 90% increase in FRET efficiency in TeTx-treated neurons (Figure 3C), meaning that synaptic activity is not required for the effect of Aβ on APP-APP interactions. In addition, a 1.5-fold increase in $[Aβ]_o$ induced by thiorphan (Th: 0.5 μM, 10 min) (Abramov et al., 2009), an inhibitor of the Aβ-degrading enzyme neprilysin, produced a 69% ± 14% increase in E_m (Figure 3B). Reducing $[Aβ]_o$ by chelating endogenously released Aβ via antibodies against Aβ decreased E_m to 57% ± 9% (HJ5.1 antibody, p < 0.01; Figure 3B) and 58% ± 9% (82E1 antibody that does not recognize a full-length APP, p < 0.05; Figure 3B), respectively. Moreover, blocking Aβ production by preincubation with γ-secretase inhibitor L-685,458 (GSI; 0.2 μM, 12 hr) reduced FRET by 51% ± 14% (p < 0.01), while addition of Aβ40 to neurons pretreated with GSI increased FRET by 101% ± 15% compared to neurons treated with γ-secretase inhibitor (p < 0.01; Figure 3B). Notably, thiorphan was not effective in neurons pretreated with γ-secretase inhibitor (Figure 3B), confirming specificity of its effect through Aβ. Finally, we measured FRET between APP^{Cer} and APP^{Cit} efficiency in neuronal cultures produced from APP/PS1 transgenic mice (Jankowsky et al., 2004), an animal model of familial AD. APP/PS1 neurons overproduce Aβ under varying patterns of neuronal activity (Dolev et al., 2013), and indeed they displayed higher FRET compared with WT neurons (p < 0.0001; Figure 3D). Moreover, the application of thiorphan caused an additional 36% FRET increase in APP/PS1 boutons (p < 0.0001; Figure 3D).

To verify these results and to determine the effect of Aβ on FRET efficiency within the fraction of interacting molecules (E_i), we utilized 2pFLIM methodology (Bacskai et al., 2003; Yasuda et al., 2006). In this method, a shortening in donor lifetime is indicative of FRET. For this purpose, we used monomeric enhanced green fluorescent protein (mEGFP) and mCherry as the donor and acceptor, respectively. mEGFP fused C terminally

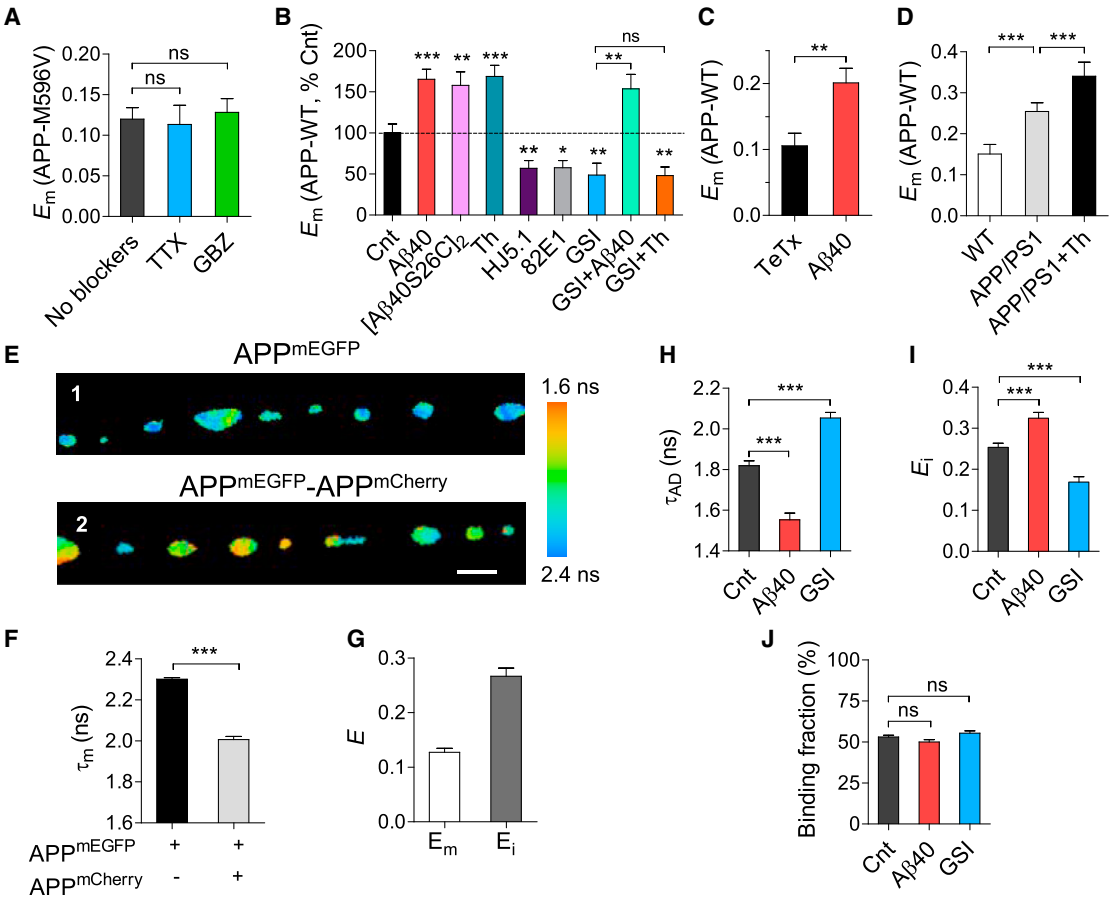

Figure 3. Aβ40 Is the Mediator of Activity-Dependent Changes in APP-APP Interactions

(A) In neurons expressing APP-M596V^{Cer} and APP-M596V^{Cit} in *APP*$^{-/-}$ neurons, FRET was not affected by either TTX (n = 32, p > 0.6) or GBZ (n = 24–31, p > 0.5). Error bars represent SEM.

(B) APP^{Cer}-APP^{Cit} E_m increased with the application of 0.5 μM thiorphan (Th: n = 60–66, p < 0.001), 100 pM Aβ40 monomers (n = 54–57, p < 0.001), and 100 pM [Aβ40S26C]$_2$ (n = 43–54, p < 0.005) and decreased with the application of HJ5.1 antibody against Aβ (10 μg/ml, n = 36–47, p < 0.01) and 82E1 antibody against Aβ (5 μg/ml, n = 19–23, p < 0.05). γ-secretase inhibitor (GSI) reduced APP^{Cer}-APP^{Cit} E_m (L-685,458, 0.2 μM: n = 27, p < 0.01). Application of thiorphan had no effect on E_m in the presence of GSI (n = 18, p < 0.01), while the addition of 100 pM Aβ40 in cultures treated by γ-secretase inhibitor increased APP^{CFP}-APP^{YFP} E_m (n = 33, p < 0.01). Error bars represent SEM.

(C) Aβ40 increased E_m in TeTx-pretreated cultures (n = 26–32, p < 0.01). Error bars represent SEM.

(D) E_m was higher in hippocampal cultures from APP/PS1 mice (n = 39–45, p < 0.001). The application of thiorphan to APP/PS1 neurons produced a further increase in APP^{Cer}-APP^{Cit} FRET (n = 24, p < 0.001). E_m measurements were performed in the presence of 0.5 μM TTX. Error bars represent SEM.

(E) APP^{GFP} fluorescence lifetime images in hippocampal boutons transfected with APP^{mEGFP} only (1) or cotransfected with APP^{mEGFP} and APP^{mCherry} (2). Scale bar, 2 μm.

(F) Decay time constant of APP^{mEGFP} in boutons expressing APP^{mEGFP} (n = 68) and APP^{mEGFP} and APP^{mCherry} (n = 95).

(G) E_m and E_i in boutons expressing APP^{mEGFP} and APP^{mCherry}.

(H) The τ_{AD} was reduced by 100 pM Aβ40 (n = 90, p < 0.0001), but increased by 0.2 μM GSI (n = 116, p < 0.0001). Error bars represent SEM.

(I) Aβ40 increased FRET efficiency within the interacting molecules (n = 90, p < 0.0001), whereas GSI reduced it (n = 116, p < 0.0001). Error bars represent SEM.

(J) The APP^{mEGFP}-APP^{mCherry} binding fraction was not affected by Aβ40 (n = 90, p > 0.4) or GSI (n = 116, p > 0.19). Error bars represent SEM.

to APP (APP^{mEGFP}) has a monoexponential lifetime decay, displaying a time constant τ_D of 2.3 ± 0.007 ns (Figures 3E and 3F). We set out to measure FRET between APP^{mEGFP} and coexpressed APP^{mCherry}. The time constant of APP^{mEGFP} was then 2.0 ± 0.01 ns (Figure 3F). In addition, fitting the fluorescence lifetime decays of the donor revealed that two donor subpopulations exist under miniature synaptic activity. One subpopulation (51.2% ± 1.4%) contains APP^{mEGFP} proteins that interact with APP^{mCherry}, resulting in a shorter fluorescent lifetime τ_{AD} of 1.7 ± 0.03 ns (Figures 3E and 3F). The remaining fraction consists of free APP^{mEGFP} proteins that display the characteristic slow monoexponential lifetime of APP^{mEGFP} monomers. FRET efficiency within the interacting molecules (E_i) was 0.26 ± 0.01 (Figure 2H) and the mean FRET efficiency (E_m) was 0.13 ± 0.07 (Figure 3G), supporting intensity-based FRET measurements.

Application of Aβ40 monomers (100 pM, 15 min) resulted in an increase of E_i from 0.25 ± 0.01 to 0.32 ± 0.01 (p < 0.0001; Figure 3I), seen as a decrease in τ_{AD}, the time constant of the fast

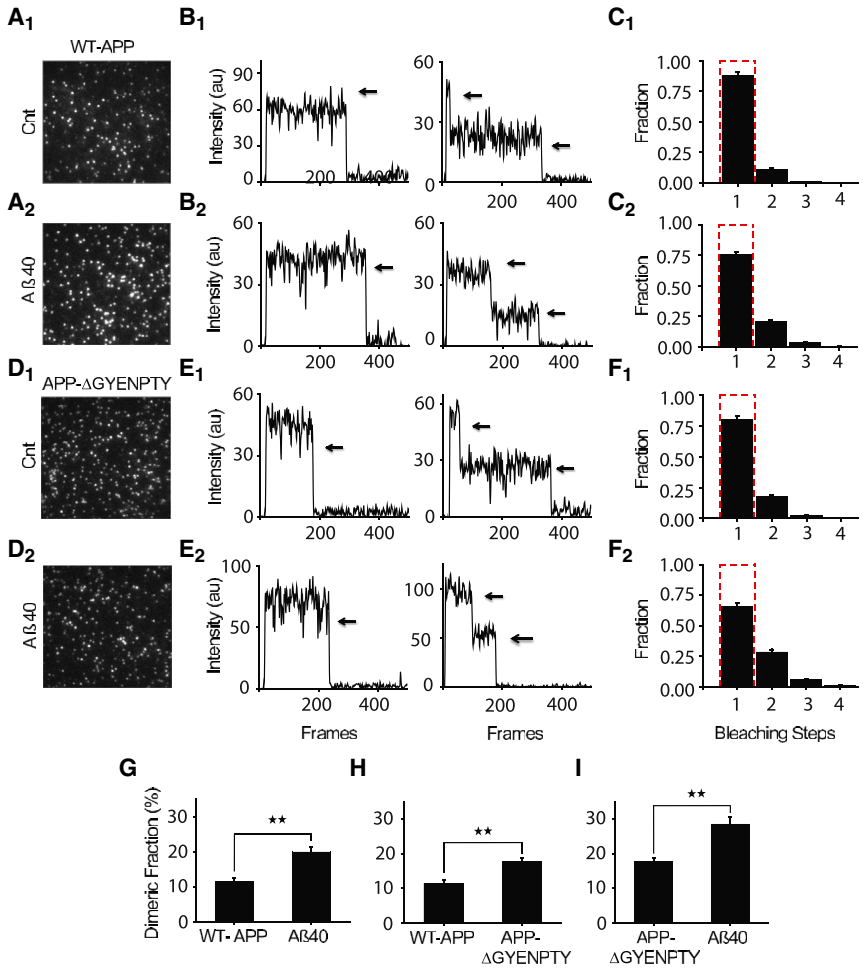

Figure 4. Aβ40 Increases the Fraction of APP Homodimers at the Plasma Membrane of *Xenopus* Oocytes

(A–C) Experiments in *Xenopus* oocytes expressing WT APP^{mEGFP}. (A) Images from representative movies showing the expression of WT APP^{mEGFP} in *Xenopus* oocytes before (Cnt; A_1) and 30 min after (A_2) the application of Aβ40 (500 nM). (B) Fluorescence intensity trace of representative spots bleaching in one and two steps indicated by arrows before (B_1) and after (B_2) Aβ40 application. (C) Bleaching step analysis of 1,353 spots before (C_1) and 1,425 spots after (C_2) the application of Aβ40. The error bars represent the counting uncertainty, and the dashed red line indicates theoretical binominal distribution for monomer with probability that mEGFP is fluorescent = 0.80. In (C), error bars represent SEM.

(D–F) Experiments in *Xenopus* oocytes expressing APP-ΔGYENPTY^{mEGFP}. (D) Images from representative movies showing expression of APP-ΔGYENPTY^{mEGFP} in *Xenopus* oocytes before (Cnt; D_1) and 30 min after (D_2) the application of Aβ40 (500 nM). (E) The fluorescence intensity trace of representative spots bleaching in one and two steps is indicated by arrows before (E_1) and after (E_2) Aβ40 application. (F) Bleaching step analysis of 1,033 spots before (F_1) and 1,040 spots after (F_2) the application of Aβ40. The error bars represent the counting uncertainty. In (F), error bars represent SEM.

(G) Aβ40 increases the dimer fraction of WT APP ($n = 23$, $p < 0.01$). Error bars represent SEM.

(H) APP dimer fraction is higher in oocytes expressing APP-ΔGYENPTY versus WT APP ($n = 13$, $p < 0.01$). Error bars represent SEM.

(I) Aβ40 increases APP-ΔGYENPT dimer fraction ($n = 14$, $p < 0.01$). Error bars represent SEM.

component of the biexponential fluorescence decay of APP^{mEGFP} coexpressed with APP^{mCherry} (from 1.82 ± 0.02 to 1.55 ± 0.03 ns, $p < 0.0001$; Figure 3H). Conversely, blocking Aβ production by GSI increased τ_{AD} to 2.05 ± 0.03 ($p < 0.0001$; Figure 3H), resulting in a decrease in the E_i to 0.17 ± 0.01 ($p < 0.0001$; Figure 3I). Neither Aβ40 nor GSI affected the relative fraction of APP^{mEGFP} proteins that interact with APP^{mCherry} ($p > 0.4$; Figure 3J), indicating that the total number of APP-APP complexes per synapse does not seem to be affected by Aβ. Altogether, these results suggest that Aβ40 is the extracellular mediator translating alterations in neuronal activity to APP-APP conformational changes.

Aβ40 Increases the Fraction of APP Homodimers at the Cytoplasmic Membrane

Next, we determined the stoichiometry of APP-APP interactions and its regulation by Aβ40 at the cytoplasmic membrane. Because spatial resolution of existing imaging methods is insufficient to address this question at small central synapses, we performed single-molecule subunit counting experiments (Ulbrich and Isacoff, 2007) on homomeric APP in the plasma membrane of *Xenopus* oocytes. Upon fusion of mEGFP to the C terminus of APP (APP^{mEGFP}) and low-density expression in oocytes, we observed sparse, well-resolved and stationary spots of green fluorescence on the plasma membrane using total internal reflection fluorescence (TIRF) microscopy (Figure 4A_1). The photobleaching of a single mEGFP is a discrete process; thus, the fluorescence intensity of a protein complex with one or several mEGFP molecules drops in a stepwise fashion, and the number of steps reflects the number of mEGFP-tagged subunits in the complex. Fluorescence intensity trajectories (e.g., Figure 4B_1) show that the majority of the APP^{mEGFP} spots bleached in one step, with smaller numbers in two steps (Figure 4C_1). Counting the bleaching steps from a total of 1,353 spots in 21 movies from nine different cells injected with APP^{mEGFP} resulted in 11.4% ± 1.1% of the APP^{mEGFP} spots that bleached in two steps (Figure 4C_1). Notably, addition of Aβ40 induced a 1.7-fold increase in the fraction of APP^{mEGFP} spots bleached in two steps to 19.9% ± 1.5% (Figures 4A_2–4C_2 and 4G), without affecting the number of APP^{mEGFP} molecules on the cell surface (Figures S5E and S5F). These results suggest that Aβ40 increases the fraction of APP homodimer complexes at the plasma membrane.

Aβ40-induced increase in the steady-state APP homodimer fraction at the cell surface may reflect dimerization of APP^{mEGFP} molecules in the plasma membrane or redistribution of

APP^{mEGFP} dimers between the intracellular compartments and the plasma membrane. Given the immobility of bright fluorescent APP^{mEGFP} spots, we explored the second possibility by deletion of the APP-GYENPTY internalization motif that inhibits clathrin-dependent APP endocytosis (Perez et al., 1999). Notably, APP-GYENPTY deletion resulted in 1.6-fold increase in the fraction of APP-ΔGYENPTY^{mEGFP} spots bleached in two steps to 17.7% ± 1.1% (Figures 4D_1–4F_1 and 4H). However, Aβ40 induced an additional 1.6-fold increase in the fraction of APP-ΔGYENPTY^{mEGFP} spots bleached in two steps (28.6% ± 2%; Figures 4D_2–4F_2 and 4I), similarly to its effect in WT APP^{mEGFP} molecules. Thus, Aβ40 increases the fraction of APP homodimers at the plasma membrane irrespective of APP internalization.

The E1 APP Domain Binds Aβ40 Monomers and Dimers

Previous studies suggested two potential APP regions that could directly interact with Aβ: (1) the Aβ homologous sequence on APP (Shaked et al., 2006) and (2) the N-terminal APP18-119 domain (Melchor and Van Nostrand, 2000; Van Nostrand et al., 2002). Because deletion of the N-terminal growth-factor-like domain (GFLD) from APP abolished the correlation between APP-APP conformation and release probability (Figure 2F), we explored direct interactions between Aβ40 monomers or Aβ40S26C dimers and the purified E1 domain of APP (Leu28-Ala198) that includes GFLD. We expressed and purified the E1 segment, as described previously (Dahms et al., 2010). Purified E1 protein was primarily monomeric, as determined by size-exclusion chromatography multiangle light scattering (Figure S6A), and exhibited a predominantly helical secondary structure (Figure S6B), consistent with the published crystal structure and indicative of proper folding. To test whether E1 directly interacts with the smallest Aβ40 species, we performed a crosslinking assay with the purified protein and Aβ40 peptide. To minimize nonspecific crosslinking, a mild crosslinker (disuccinimidyl suberate [DSS]) was used at a low concentration (50 μM). Following reaction of E1 protein with different concentrations of monomeric Aβ40 in the presence of DSS, crosslinked products were resolved by SDS-PAGE and detected by the 6E10 antibody against the Aβ40 N terminus (Figure 5A). Complex formation was detected between E1 (~21 kDa) and monomeric Aβ40, revealing a 25 kDa band (lane 1). Notably, higher concentrations of monomeric Aβ40 yielded an additional 29 kDa band, corresponding to the complex of E1 with two molecules of Aβ40 (lanes 2 and 3), suggesting that the binding to E1 may induce Aβ40 dimerization. Increasing the E1 concentration revealed increased crosslinking between E1 and either monomeric or dimeric Aβ40 (lane 4). No complex formation was detected in the absence of E1 (lane 5), Aβ40 (lane 6), or DSS (lane 7). Moreover, Aβ40 did not dimerize in the absence of E1. Underscoring the specificity of this interaction, no crosslinking was detected between Aβ40 and nonrelated purified protein Tim44 (lane 11). Crosslinking of E1 and Aβ40S26C dimers (Figure S2) yielded a dominant 29 kDa band (Figure 5A, lane 8), consistent with E1:$[Aβ S26C]_2$ complex. Notably, the 29 kDa band did not appear in the absence of E1 (lane 9) or DSS (lane 10). Together, these results support direct and specific E1:Aβ40 interaction and may hint that the binding to E1 induces some degree of Aβ40 oligomerization.

Next, we asked whether Aβ40 binds to endogenous APP expressed in neurons. For this purpose, hippocampal cultures were incubated with biotinylated monomeric Aβ40 (Aβ40-biotin) and then fixed and visualized with alkaline phosphatase conjugated to streptavidin using nitro-blue tetrazolium chloride/5-bromo-4-chloro-3'-indolyl phosphate p-toluidine salt dye for substrate as shown in Figure 5B. Saturable, concentration-dependent Aβ40-biotin binding to WT hippocampal neurons was detected (Figure 5C). Given the wide variety of proposed Aβ binding candidates, we quantitated the contribution of APP to the Aβ40-biotin signal detected in WT neurons. Notably, the fraction of the bound Aβ40-biotin was reduced by 48% in $APP^{-/-}$ neurons in comparison to those in WT neurons ($p < 0.0001$; Figure 5D). Moreover, preincubation of WT cultures with the 22C11 antibody raised against APP residues 66–81, the potential Aβ binding epitope, reduced the bound Aβ40-biotin fraction by 46% ($p < 0.001$; Figure 5D), consistent with the 22c11 antibody preventing Aβ40-biotin binding to APP. Notably, neither 22c11 antibody nor Aβ40 affected the abundance of APP molecules at the cell surface as estimated by TIRF microscopy ($p > 0.2$; Figures S5E and S5F). Taken together, these results suggest that neuronal APP represents a bona fide candidate for association with monomeric Aβ40 and dimeric Aβ40S26C species.

APP-GFLD Is Critical for Aβ-Induced Changes in APP-APP Interactions

To explore whether the N-terminal APP domain is essential for the Aβ-induced changes in APP-APP interactions, we tested the deletion of the N-terminal GFLD (Rossjohn et al., 1999) of APP (Δ22–128; APP-ΔGFLD) on FRET between APP molecules (Figure 6A). The basal FRET levels were not significantly different between APP-ΔGFLD and APP-WT proteins ($p > 0.1$; Figure 6B). However, in APP-ΔGFLD molecules, FRET lost its sensitivity to all manipulations aimed at changing $[Aβ]_o$ ($p > 0.4$; Figures 6C, S5C, and S5D), suggesting that the APP-GFLD is required for Aβ-induced APP-APP conformational changes. It is noteworthy that the GFLD deletion abolished the observed correlation between FRET efficiency and FM dye release upon stimulation (Spearman $r = 0.2$, $p = 0.5$; Figure 2F_2). Moreover, addition of the 22c11 antibody raised against the APP66-81 region within the APP-GFLD increased the basal FRET ($p < 0.01$; Figure 6B) and prevented further FRET modulation by TTX and Aβ40 ($p > 0.4$; Figure 6D).

Next, we examined the importance of the Aβ homologous sequence on APP, which has been suggested to directly bind Aβ (Shaked et al., 2006), by replacing it with the cognate region from APLP2, the sequence of which is divergent from APP (APP-APLP2; Figure 6A). Both basal FRET (Figure 6B) and its regulation by TTX and Aβ40 (Figure 6E) were preserved in the chimeric APP-APLP2 protein, thus ruling out the Aβ homologous region in APP as essential for Aβ-dependent modulation of APP-APP interactions. These experiments suggest that the GFLD of APP constitutes the molecular determinant that regulates Aβ-mediated, activity-dependent modulation of conformational changes within APP homodimers.

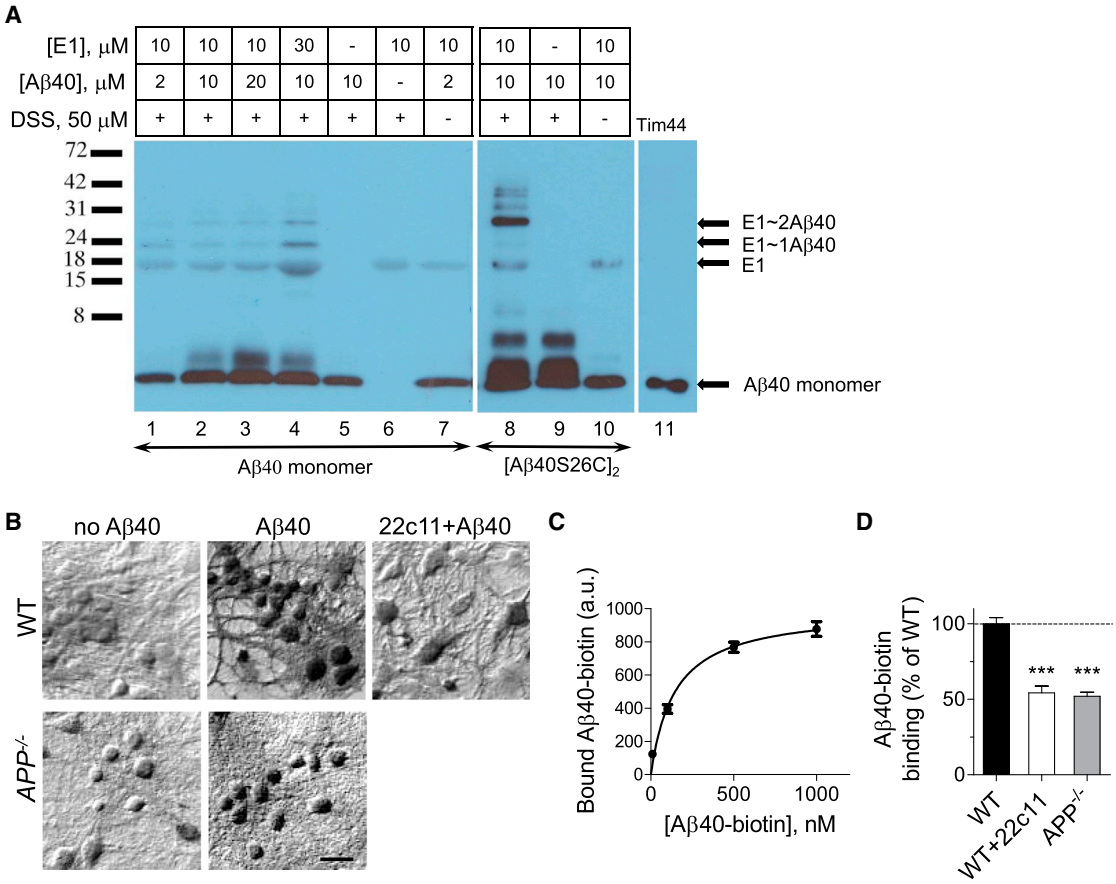

Figure 5. Aβ40 Monomers and Dimers Bind to APP

(A) A complex between E1 and Aβ40 at different concentrations was formed by incubating the proteins for 10 min and subsequent addition of DSS (lanes 1–4). Crosslinked products were analyzed by SDS-PAGE followed by western blotting with 6E10 antibody. Control experiments are shown in lanes 5–7. E1 and $[Aβ40S26C]_2$ were incubated to allow complex formation under the same conditions as monomeric Aβ40 (lane 8). The complex formed correlates with E1 and $[Aβ40S26C]_2$. Control experiments for the dimeric crosslinking reaction are shown in lanes 9 and 10. Lane 11 is a negative control, replacing E1 with an unrelated protein, Tim44 (44 kDa). SDS-PAGE was performed under reducing conditions.

(B) Representative images demonstrating binding of monomeric Aβ40-biotin as visualized by alkaline phosphatase conjugated to streptavidin. Aβ40-biotin (500 nM) specifically binds to hippocampal neurons (14 DIV) in WT culture. The Aβ40-biotin binding was reduced in $APP^{-/-}$ neurons and by preincubation of WT neurons with 22C11 antibody against the APP N terminus. Scale bar, 30 μM

(C) Dose dependence of Aβ40-biotin binding to hippocampal neurons (n = 80–111). Error bars represent SEM.

(D) Preincubation of WT culture with 22C11 antibody against APP decreased Aβ40-biotin binding to WT neurons by 46% (n = 110–167). Binding of Aβ40-biotin to $APP^{-/-}$ neurons was reduced by 48% compared to binding in WT neurons (n = 324). Error bars represent SEM.

APP-GFLD Is Required for the Aβ-Mediated Presynaptic Enhancement

Because Aβ mediates enhancement of basal synaptic vesicle release, we next examined whether it does so through the APP-GFLD. First, we compared the effect of Aβ on synaptic vesicle recycling evoked by 0.2 Hz stimulation using FM1-43 dye in functional boutons of $APP^{-/-}$ neurons versus boutons expressing APP-WT or APP-ΔGFLD proteins. While Aβ40 had no effect on vesicle recycling in $APP^{-/-}$ boutons ($p > 0.7$; Figures 1E–1I and 6G), its effect was rescued by expression of the CFP-tagged APP-WT in $APP^{-/-}$ neurons ($p < 0.001$; Figures 6F, 6G, and S7A). Moreover, Aβ caused a 79% increase of the presynaptic strength in the APP-APLP2 expressing boutons ($p < 0.0001$; Figures 6G and S7A), suggesting that the Aβ cognate APP's domain is not essential for Aβ-mediated presynaptic enhancement. In contrast, Aβ completely lost its ability to increase synaptic vesicle turnover in neurons expressing APP-ΔGFLD ($p > 0.2$; Figures 6F, 6G, and S7A) or APP-KK, which is unable to reach the cell surface ($p > 0.3$; Figures 6G and S7A), further supporting our hypothesis that APP serves as a cell-surface receptor. Notably, the application of 22c11 antibody, which binds to the APP-GFLD and promotes APP-APP interactions, increased synaptic vesicle recycling in WT neurons ($p < 0.0001$; Figure 6H), mimicking the effect of Aβ40. Addition of Aβ40 in 22c11-pretreated neurons did not produce further enhancement of the presynaptic strength ($p > 0.2$; Figure 6H), while the boiled 22c11 did not interfere with the Aβ40 effect (Figure S7B). Thus, our results demonstrate that the

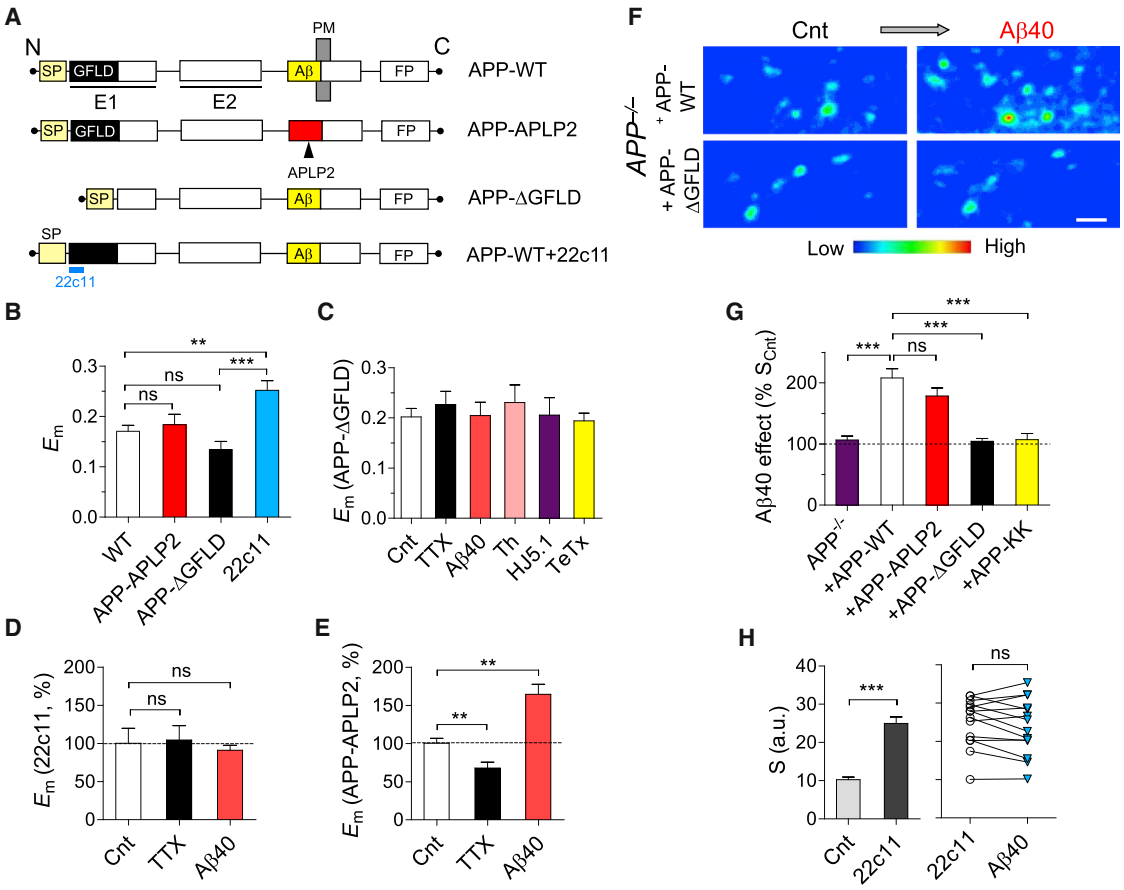

Figure 6. APP-GFLD Is Required for Aβ-Mediated APP-APP Conformational Changes and Presynaptic Enhancement

(A) Schematic illustration of the subdomains in the full and modified APP protein. All the constructs used for FRET detection were fused to Cit or Cer and the C terminus.

(B) E_m was not significantly changed by deletion of GFLD (n = 62, p > 0.05) or replacing the Aβ domain by mAPLP2 homolog (n = 28, p > 0.6) compared to APP-WT E_m levels (n = 106). Preincubation with 22C11 APP antibody elevated APP-WT E_m (n = 68, p < 0.01). E_m measurements were performed in the presence of 0.5 μM TTX. Error bars represent SEM.

(C) APP-ΔGFLD^{Cer}-APP-ΔGFLD^{Cit} FRET (n = 85, p > 0.6) was not sensitive to TTX (n = 38, p > 0.6), 100 pM Aβ40 (n = 30, p > 0.8), 0.5 μM thiorphan (n = 16, p > 0.5), HJ5.1 antibody against Aβ (n = 16, p > 0.8), and TeTx (n = 40, p > 0.5). Error bars represent SEM.

(D) APP^{Cer}-APP^{Cit} FRET in culture preincubated with 22C11 APP antibody was not sensitive to TTX (n = 13–17, p > 0.8) and 100 pM Aβ40 (n = 60–72, p > 0.4). Error bars represent SEM.

(E) TTX decreased APP-APLP2^{Cer}-APP-APLP2^{Cit} FRET by 33% (n = 28, p < 0.01), whereas 100 pM Aβ40 increased FRET by 65% (n = 45, p < 0.01). Error bars represent SEM.

(F) Representative ΔF_{FM1-43} images before and 15 min after application of 100 pM Aβ40 in *APP*$^{-/-}$ neurons transfected with either APP-WT^{CFP} or APP-ΔGFLD^{CFP}. Fluorescence intensities (arbitrary units) are coded using a pseudo-color transformation. Scale bar, 2 μM. Error bars represent SEM.

(G) Average magnitude of the effects produced by 100 pM Aβ40 on *S* in *APP*$^{-/-}$ neurons transfected with different APP mutants (the same data as in B). Aβ40 had no effect on S in *APP*$^{-/-}$ neurons transfected with Cer only (n = 20, p > 0.7), APP-KK (n = 13, p > 0.3), or APP-ΔGFLD (n = 33, p > 0.5). Aβ40 increased S in APP$^{-/-}$ neurons transfected with APP-WT (n = 38, p < 0.0001) and APP-APP-mAPLP2 (n = 12, p < 0.0001). Error bars represent SEM.

(H) Preincubation with 22c11 antibody (5 μg/ml, 2 hr) increased presynaptic strength in WT hippocampal neurons (n = 14, p < 0.0001). Aβ40 (100 pM) was ineffective (n = 14, p > 0.2) in 22c11-pretreated WT neurons. Error bars represent SEM.

APP-GFLD is essential for the Aβ-mediated presynaptic enhancement.

APP/G_o Protein Signaling Complex Mediates Presynaptic Enhancement by Aβ

We asked how APP-APP conformational changes are transduced to augment synaptic release probability. Previous studies proposed that the APP forms a complex with G_o protein (Nishimoto et al., 1993; Swanson et al., 2005). Thus, we explored whether $G_{i/o}$ proteins mediate Aβ-induced presynaptic enhancement by testing the effect of pertussis toxin (PTX), which catalyzes the ADP-ribosylation of α subunits of the heterotrimeric $G_{i/o}$ protein and uncouples it from the receptor, on the effect of thiorphan or Aβ40 on synaptic vesicle release. We found that PTX profoundly reduced the effects of both thiorphan and Aβ40 on synaptic vesicle release (p < 0.0001; Figure 7A).

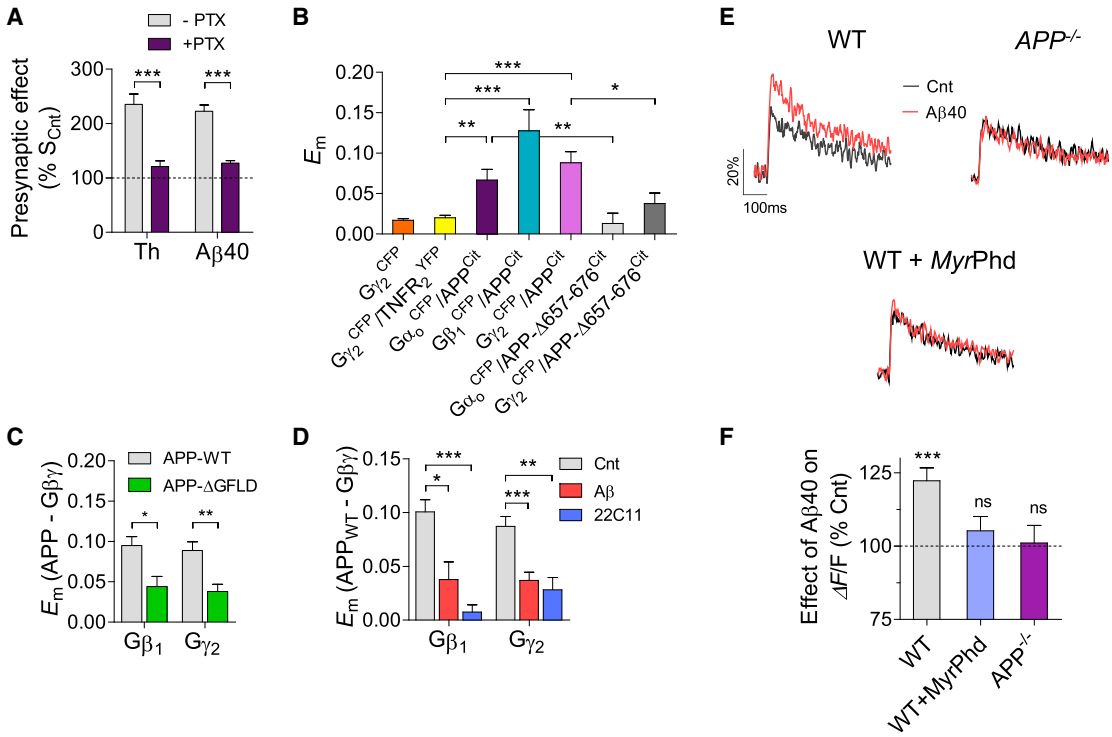

Figure 7. $G_{i/o}$ Protein Mediates Aβ40-Induced Enhancement of Presynaptic Calcium Flux and Vesicle Release

(A) PTX pretreatment abolished enhancement of synaptic vesicle release caused by 0.5 μM thiorphan (N = 9, $p < 0.001$) or by 100 pM Aβ40 (N = 9–12, $p < 0.01$). Error bars represent SEM.

(B) FRET was detected between APP^{Cit} and $G\alpha_o{}^{CFP}$ (n = 27), APP^{Cit} and $G\beta_1{}^{CFP}$ (n = 25), and APP^{Cit} and $G\gamma_2{}^{CFP}$ (n = 66) proteins under miniature synaptic activity at single hippocampal boutons. Lower E_m was monitored between APP-Δ657-676^{Cit} and $G\alpha_o{}^{CFP}$ (n = 24) and APP-Δ657-676^{Cit} and $G\gamma_2{}^{CFP}$ (n = 15). To verify FRET specificity, E_m was measured between the CFP-tagged proteins of interest and nonrelated $TNFR_2{}^{YFP}$. Error bars represent SEM.

(C) Deletion of APP-GFLD reduced APP^{Cit}-$G\gamma_2{}^{CFP}$ FRET by 57% (n = 43 - 46, $p < 0.01$) and APP^{Cit}-$G\beta_1{}^{CFP}$ FRET by 54% (n = 24–31, $p < 0.05$). Error bars represent SEM.

(D) Aβ40 reduced APP^{Cit}-$G\gamma_2{}^{CFP}$ FRET by 58% (n = 74–82, $p < 0.0001$) and APP^{Cit}-$G\beta_1{}^{CFP}$ FRET by 62% (n = 16–25, $p < 0.05$). 22c11 reduced APP^{Cit}-$G\gamma_2{}^{CFP}$ FRET by 68% (n = 20–32, $p < 0.0001$) and APP^{Cit}-$G\beta_1{}^{CFP}$ FRET by >90% (n = 44–56, $p < 0.01$). Error bars represent SEM.

(E) Spike-dependent presynaptic Ca^{2+} transients (Δ*F*/*F*) evoked by 0.2 Hz stimulation in WT, $APP^{-/-}$, and *Myr*Phd-expressing WT neurons before and after Aβ40 application. Ca^{2+} transients were quantified before (black) and after (red) Aβ40 application (average of ten traces).

(F) Average data on Aβ40-induced modification in Ca^{2+} transients normalized to control in WT (n = 48, $p < 0.001$), $APP^{-/-}$ (n = 28, $p > 0.8$), and *Myr*Phd-expressing (n = 21, $p > 0.2$) boutons. Error bars represent SEM.

Next, we explored whether APP closely interacts with G_o proteins in presynaptic boutons by measuring possible FRET between the tagged APP and G_o protein subunits. FRET was tested between APP^{Cit} and the CFP-tagged $G\alpha_o$ subunit, where CFP is internally inserted after E94 ($G\alpha_o{}^{CFP}$), $G\gamma_2$ G protein subunit N-terminally tagged to CFP ($G\gamma_2{}^{CFP}$), and $G\beta_1$ G protein subunit N-terminally tagged to CFP ($G\beta_1{}^{CFP}$) (Laviv et al., 2011). Quantitative analysis of FRET signals across different boutons revealed E_m of 0.07 ± 0.01 for APP^{Cit}-$G\alpha_o{}^{CFP}$, 0.12 ± 0.02 for APP^{Cit}-$G\beta_1{}^{CFP}$, and 0.09 ± 0.01 for APP^{Cit}-$G\gamma_2{}^{CFP}$ proteins (Figure 7B). Notably, deletion of the APPHis657-Lys676 cytoplasmic domain, which has been proposed to mediate APP's interaction with G_o protein (Nishimoto et al., 1993; Okamoto et al., 1995), significantly reduced APP FRET with $G\alpha_o{}^{CFP}$ and $G\gamma_2{}^{CFP}$ (APP-Δ657–676; Figure 7B). The deletion of the APP-GFLD reduced APP FRET with $G\beta_1{}^{CFP}$ and $G\gamma_2{}^{CFP}$ (Figure 7C). The application of Aβ40 or 22c11 reduced APP^{Cit}-$G\gamma_2{}^{CFP}$ and APP^{Cit}-$G\beta_1{}^{CFP}$ FRET (Figure 7D), pointing to a modulation of APP-$G\beta_1\gamma_2$ interactions by Aβ in hippocampal boutons. Taken together, these results suggest that APP forms a signaling complex with G_o proteins to mediate Aβ-induced presynaptic enhancement at presynaptic boutons.

Finally, we examined whether Aβ potentiates vesicle release by increasing presynaptic Ca^{2+} flux. Presynaptic Ca^{2+} transients evoked by low-frequency stimulation were measured by high-affinity fluorescent calcium indicator Oregon Green 488 BAPTA-1 AM. Aβ40 had no effect on resting Ca^{2+}-dependent fluorescence, whereas it increased the size of action-potential-dependent fluorescence transients (Δ*F*/*F*; Figure 7E). Aβ40 induced a potentiation of presynaptic Ca^{2+} transients by ~22% in WT neurons ($p < 0.001$; Figures 7E and 7F), whereas it did not significantly affect Ca^{2+} transients in $APP^{-/-}$ neurons ($p > 0.6$; Figures 7E and 7F). Moreover, Aβ40 effect on Ca^{2+} flux was prevented by transfection of WT neurons with the membrane-targeted Gβγ scavenger N-myristoylated phosducin (Laviv et al., 2011) (*Myr*Phd; $p > 0.2$; Figures 7E and 7F),

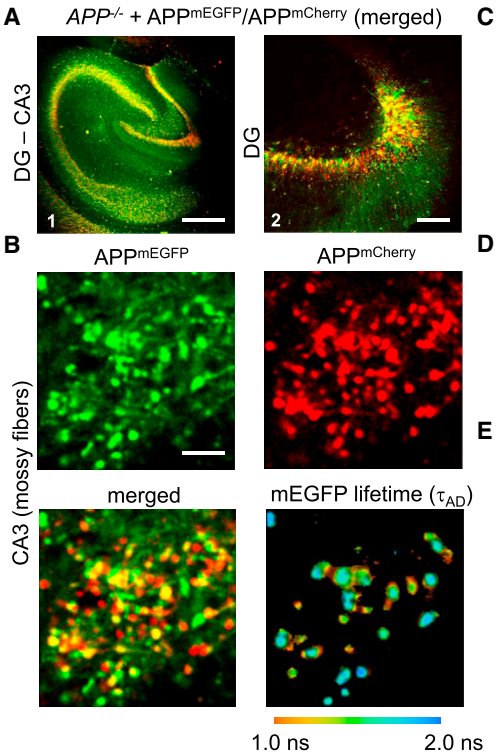

Figure 8. Aβ40 Promotes APP-APP Interactions at Mossy Fiber Terminals in Acute Hippocampal Slices

(A) APP^{mEGFP} and $APP^{mCherry}$ expression in the CA3 and dentate gyrus (DG) of $APP^{-/-}$ mice injected with lentiviral vectors to the DG (A1). Zoom in to the DG expression (A2). Scale bars represent 0.5 mm (A1) and 0.1 mm (A2).

(B) In the CA3 area, mEGFP and mCherry fluorescence is localized in the stratum lucidum where the mossy fibers project. Mossy fiber terminals positive for mEGFP and mCherry fluorescence and color-coded APP^{mEGFP} decay constant. Scale bar, 10 μm.

(C–E) Left: application of Aβ40 (20 nM, 30 min, n = 58, seven slices from three mice) in hippocampal slices of $APP^{-/-}$ mice expressing APP^{mEGFP} and $APP^{mCherry}$ accelerated the decay constant of the interacting molecules (C; τ_{AD}, $p < 0.01$) and increased FRET efficiency between APP^{mEGFP} and $APP^{mCherry}$ coexpressed at mossy fibers (D; E_i, $p < 0.01$) but did not alter the fraction of interacting APP^{mEGFP} and $APP^{mCherry}$ (E; $p = 0.3$). Right: thiorphan treatment (20 μM, 30 min, n = 94, four slices from two mice) accelerated τ_{AD} (C; $p < 0.0001$) and increased E_i (D; $p < 0.0001$) but did not affect the binding fraction (E; $p = 0.48$). Error bars represent SEM.

indicating an involvement of Gβγ subunits in this presynaptic modulation.

Aβ Regulates Presynaptic APP-APP Interactions in Hippocampal Tissue

Finally, we extended the scope of our in vitro and cell-culture study to acute hippocampal slices to gain information on the regulation of presynaptic APP-APP interactions by extracellular Aβ levels in native brain tissue. We generated two lentiviral (LV) vectors containing APP^{mEGFP} and $APP^{mCherry}$ driven by the CaMKII promoter for selective expression in excitatory neurons. Concentrated viral particles of both LV vectors were injected in the dentate gyrus (DG) of the hippocampal formation using a stereotactic apparatus. After 1–2 months, the hippocampi of the injected adult mice were sliced and imaged. First, we injected APP^{mEGFP} and $APP^{mCherry}$ LVs in the DG of $APP^{-/-}$ mice. Half of the infected granule cells coexpressed APP^{mEGFP} and $APP^{mCherry}$ in the somatodendritic and axonic compartments of the DG (Figures 8A and 8B). In the CA3 area (Figure 8B), fluorescence was mainly observed in the stratum lucidum where the mossy fibers project and make synapses with postsynaptic cells. Tagged APP molecules appeared mainly as punctate with a diameter of 2–5 μm that are reminiscent of the giant and small mossy terminals (Acsády et al., 1998). Using 2pFLIM, we measured the lifetime of APP^{mEGFP} at the mossy terminals coexpressing $APP^{mCherry}$. The lifetime decay of the interacting proteins was 1.94 ± 0.04 ns (Figure 8C), 19% lower than the one measured at terminals expressing APP^{mEGFP} alone (2.4 ± 0.02 ns). These data indicate an interaction between APP^{mEGFP} and $APP^{mCherry}$ molecules at mossy terminals, corresponding to 0.24 ± 0.02 FRET efficiency (Figure 8D). Application of monomeric Aβ40 (20 nM, 30 min) led to a decrease in the lifetime decay of APP^{mEGFP} to 1.74 ± 0.07 ns in the terminals coexpressing $APP^{mCherry}$ ($p < 0.0001$; Figure 8C), resulting in a 42% increase in FRET efficiency to 0.34 ± 0.03 ($p < 0.0001$; Figure 8D). Similar to the data in cultured neurons, the fraction of interacting molecules per synapse was not changed by Aβ40 application ($p = 0.3$; Figure 8E).

Next, we injected APP^{mEGFP} and $APP^{mCherry}$ LVs in the DG of WT mice. To increase the extracellular levels of endogenous Aβ, we inhibited its neprilysin-mediated degradation by thiorphan. Application of thiorphan (20 μM, 30 min) lead to a decrease in the lifetime decay of APP^{mEGFP} from 1.89 ± 0.03 ns to 1.71 ± 0.04 ns in the terminals coexpressing $APP^{mCherry}$ ($p < 0.0001$; Figure 8C), resulting in a 34% increase in FRET efficiency to 0.39 ± 0.02 ($p < 0.0001$; Figure 8D) while not affecting the fraction of interacting molecules per synapse ($p > 0.4$; Figure 8E). These results indicate that extracellular Aβ promotes presynaptic APP-APP interactions in hippocampal tissue.

DISCUSSION

Elucidating the mechanisms by which Aβ peptides regulate synaptic transmission is essential for understanding normal synaptic function as well as early synaptic dysfunctions in AD. In the current study, we found that APP binds Aβ40 monomers and dimers, increases the fraction of APP homodimers at the plasma membrane, and induces activity-dependent APP-APP conformational changes. APP homodimer activation, in turn,

leads to structural rearrangements within the presynaptic APP/G_o protein signaling complex, resulting in enhancement of presynaptic calcium flux and, thus, synaptic vesicle exocytosis. We identified the APP growth-factor-like domain as a critical determinant of Aβ40-induced changes in APP-APP interactions and release probability. Collectively, our data delineate APP homodimer as a presynaptic receptor that translates local changes in the extracellular Aβ levels to modulation of synaptic release probability. This mechanism may maintain basal neurotransmitter release under physiological conditions and initiate hippocampal hyperactivity under pathological conditions, promoting a positive feedback loop leading to extracellular Aβ accumulation.

Activity Promotes APP-APP Interactions at Hippocampal Boutons

Previous studies suggest that APP can form homodimers and higher-order oligomers in heterologous expression systems (Eggert et al., 2009; Kaden et al., 2009; Munter et al., 2007; Scheuermann et al., 2001) and in brain homogenates (Bai et al., 2008). Moreover, APP homodimerization seems to affect Aβ generation: dimerization strength in the transmembrane GxxxG APP domain within the Aβ sequence regulates the γ-secretase cleavage of APP, increasing the Aβ42/40 ratio (Munter et al., 2007). However, induced dimerization at the APP C terminus reduced the total Aβ production (Eggert et al., 2009). While the structure and biological function of APP have been extensively explored, several key questions remain unresolved to date. First, do APP homodimers, localized at presynaptic compartments, undergo modulation by endogenously released Aβ species? Second, does neuronal activity regulate APP-APP interactions in neurons? Third, what is the effect of APP-APP interactions on synaptic function?

Utilizing FRET spectroscopy and 2pFLIM-FRET, we were able to monitor APP-APP interactions at individual presynaptic boutons of live neurons in hippocampal cultures and acute slices. The specific intermolecular FRET between APP^{Cer} and APP^{Cit} was detected not only in WT neurons but also between the tagged APP molecules expressed in $APP^{-/-}$ neurons (Figure 2E). While FRET methodology allows deciphering intermolecular interactions in small subcellular structures such as synapses (Laviv et al., 2010), it requires expression of fluorescent-tagged proteins, raising the question of the possible effects of protein overexpression. However, the following facts suggest that homophilic APP interactions occur at physiologically relevant APP levels. First, the level of the tagged APP expression in the axons of $APP^{-/-}$ neurons was similar to the endogenous APP level in WT neurons (Figure S3). Second, the functional effect of Aβ40 in $APP^{-/-}$ neurons expressing the tagged APP-WT was comparable to those induced by Aβ40 in WT neurons. The observed intermolecular APP-APP FRET displayed considerable variability among boutons (Figure 2F_2). This heterogeneity may derive from differences in the APP length (processed and full), local mechanisms regulating APP-APP interactions or inter-synapse differences in the microenvironment. Indeed, APP-APP interactions display robust, rapid, and bidirectional regulation by synaptic activity. Basal APP homodimerization did not require synaptic activity, in agreement with an earlier study suggesting that APP dimers can form in the ER shortly after its synthesis (Scheuermann et al., 2001). In contrast, APP-APP interactions were modulated by spiking rate, Ca^{2+} flux through presynaptic voltage-gated calcium channels, and synaptic release probability (Figure 2), while neuronal activity did not affect FRET between APP-KK proteins containing an ER retention signal. We conclude that the fraction of APP homodimers localized at the cytoplasmic membrane is regulated by activity-dependent conformational modifications.

Aβ as the Mediator of Activity-Dependent APP-APP Interactions

Spiking rate and synaptic activity could affect APP-APP conformation either (1) by directly changing the membrane potential or (2) through activity-dependent release of a putative mediator. This second possibility, where extracellular Aβ40 serves as the mediator inducing APP-APP structural changes, is supported by the following evidence: (1) Aβ40 monomers and Aβ40S26C dimers directly bind to the E1 domain of the APP; (2) Aβ40 increases the fraction of APP dimers at the plasma membrane and FRET between APP molecules in heterologous expression systems; (3) activity-dependent FRET changes were abolished in neurons lacking Aβ production following introduction of the APP-M596V mutation preventing β-secretase cleavage; and (4) FRET was altered by direct regulation of extracellular Aβ levels. Specifically, both antibody against Aβ that does not recognize full-length APP and γ-secretase inhibitor reduced FRET. On the other hand, inhibition of Aβ degradation by thiorphan, the addition of Aβ40 monomers or Aβ40S26C dimers, and an increase in Aβ production by APP/PS1 mutations boosted FRET between APP molecules. Notably, the GFLD of APP constitutes the molecular determinant required the activity-induced and Aβ-mediated APP-APP conformational changes.

What are the Aβ species that induce an increase in glutamate release? Our data provide evidence that Aβ40 monomers and dimers, the smallest Aβ species, regulate presynaptic function through activation of APP homodimers in hippocampal boutons. This finding highlights a previously neglected role of Aβ40 monomers in synaptic dysfunctions and is in contrast to an earlier study in which cell media containing Aβ monomers and SDS-stable low-n oligomers had no effect on presynaptic function estimated by paired-pulse ratio (Townsend et al., 2006). However, Aβ dimers (from human brain as well as synthetic cross-linked dimers) were suggested to represent the principal and the smallest species that cause postsynaptic depression of glutamatergic transmission via loss of dendritic spines, blockade of long-term potentiation, and increase in long-term synaptic depression (Shankar et al., 2008). Notably, later biophysical characterization of Aβ40S26C dimers point to the fact that it is not dimers per se but rather protofibrils that mediate this activity (O'Nuallain et al., 2010). Thus, it seems that the smallest Aβ species, monomers and dimers, enhance presynaptic function, while higher-molecular-weight prefibrillar assemblies may initiate postsynaptic depression in excitatory synaptic connections.

APP Homodimer as a Presynaptic Aβ40 Receptor

Does the APP homodimer, similar to the receptor tyrosine kinases, trigger signal transduction through ligand-promoted

receptor dimerization? Although the APP structure is reminiscent of other cell-surface receptors involved in signal transduction (Kang et al., 1987), the role of APP as a bona fide surface receptor has remained speculative. Physical interaction between pathological Aβ levels/conformations and APP was proposed a decade ago as a mechanism inducing neuronal death in AD (Lorenzo et al., 2000; Shaked et al., 2006; Van Nostrand et al., 2002). However, in addition to APP, a wide range of other putative Aβ receptors can induce neurotoxicity, suggesting biophysical and structural heterogeneity of toxic Aβ species or, alternatively, nonspecific interactions between a mixture of toxic peptides with cellular membranes and proteins (Benilova et al., 2012).

Our data highlight the role of APP as a bone fide surface Aβ40 receptor that triggers a signaling cascade leading to augmentation of synaptic vesicle release in hippocampal neurons. The full-length APP may undergo cleavage by either α- or β-secretase, resulting in the shedding of large extracellular portions of APP termed APPsα or APPsβ, respectively. Notably, β-secretase mainly cleaves APP in the endosomal pathway (Koo and Squazzo, 1994), while ADAM10 α-secretase resides in the postsynaptic densities (Marcello et al., 2007). Thus, the presynaptic plasma membrane appears to be the primary location of unprocessed APP molecules that transduce changes in Aβ levels to synaptic strength.

How does Aβ exert its presynaptic effect? Following secretion, Aβ forms the Aβ:APP complex that triggers APP-APP conformational changes, leading to an increases in the presynaptic Ca^{2+} flux and subsequent potentiation of synaptic vesicle release. Because Aβ-mediated enhancement of Ca^{2+} flux or vesicle release was prevented by either PTX or Gβγ scavenger, we concluded that $G_{i/o}$ proteins are involved in this signaling cascade. Moreover, we observed a close interaction between APP molecules and $G\alpha_o\beta_1\gamma_2$ protein subunits at individual presynaptic boutons, suggesting a formation of the signaling complex that is undergoing conformational changes by the smallest Aβ40 species. Reduction in APP/G_o protein interactions at various stages of cognitive decline in AD patients (Shaked et al., 2009) indicates the importance of the APP/G_o protein signaling complex in AD progression.

Synapse Hyperactivity and Alzheimer's Disease

Numerous human and animal studies suggest the role of cortical and hippocampal hyperactivity in AD pathogenesis. High default activity in specific brain regions of young adults correlates with the spatial pattern of amyloid depositions in elderly individuals with AD (Buckner et al., 2005). Aberrant neuronal activity in the hippocampus and cortex has been reported in humans with mild cognitive impairment (Bakker et al., 2012), in AD patients (Vossel et al., 2013), and in familial AD transgenic animal models (Busche et al., 2008; Palop et al., 2007; Verret et al., 2012). Various molecular and cellular mechanisms may contribute to brain hyperactivity in AD. For example, deficits in parvalbumin-positive interneurons have been proposed to underlie abnormalities in network synchrony and cognitive functions in APP transgenic mice (Verret et al., 2012). Young APP/PS1 transgenic mice exhibit increased basal glutamate release in CA3-CA1 hippocampal connections (Dolev et al., 2013) and increased spontaneous Ca^{2+} transients in vivo in pyramidal neurons in the CA1 region of hippocampus (Busche et al., 2012). Notably, hyperactivity of pyramidal neurons has been reported to occur before neuronal depression and plaque deposition in the hippocampus of APP/PS1 mice (Busche et al., 2012). Based on the current work, we propose that increases in the extracellular level of Aβ monomers and dimers in the early stages of AD development may augment signaling via APP homodimers, leading to hyperactivity of excitatory hippocampal synapses (Figure S8). Potentiation of synaptic vesicle release in turn causes a subsequent increase in Aβ40 production and release (Cirrito et al., 2005; Dolev et al., 2013), leading to a positive feedback loop between the extracellular Aβ concentration and basal glutamate release. Under physiological conditions, an increase in Aβ-mediated APP homodimerization may induce a feedback inhibition of Aβ production (Eggert et al., 2009) to maintain steady-state Aβ levels and basal glutamate release. Disruption of this negative feedback loop by genetic- or experience-dependent factors may cause a gradual increase in the extracellular levels of Aβ monomers and dimers during the early AD stages, leading to excessive activation of APP homodimers at the plasma membrane and subsequent hyperactivity of excitatory hippocampal synapses. The described presynaptic hyperactivity may initiate neural dysfunctions by two possible ways. First, it may cause deficits in short-term synaptic plasticity (Abramov et al., 2009). Second, it may facilitate the kinetics of Aβ oligomerization and thus depress synapses and induce synapse loss. Such an Aβ-induced synaptic reorganization may promote homeostasis of synaptic output across the dendrites but reduce the ability of synaptic networks to undergo experience-dependent modifications. It remains to be seen whether excessive activation of APP homodimers by Aβ emerges as the first molecular step contributing to hippocampal hyperactivity in the most frequent, sporadic AD.

EXPERIMENTAL PROCEDURES

Primary Hippocampal Cultures and Acute Hippocampal Slices

Primary cultures of CA3-CA1 hippocampal neurons were prepared from newborn Sprague-Dawley rats and from $APP^{-/-}$ (Zheng et al., 1995) and corresponding WT mice (C57BL/6J background) on postnatal days 0–2, as described previously (Abramov et al., 2009). Acute hippocampal slices were prepared from 2- to 3-month-old $APP^{-/-}$ and BALB/c mice 1 month after lentivirus injections. All animals were kept in a normal light/dark cycle (12 hr/12 hr) with three animals per cage. Coronal slices (400 μm) of hippocampus were prepared as described before (Abramov et al., 2009). Slices were transferred to a submerged recovery chamber at room temperature containing oxygenated (95% O_2 and 5% CO_2) artificial cerebrospinal fluid (ACSF) for 1 hr before the experiment. The ACSF contained, in mM, NaCl, 125; KCl, 2.5; $CaCl_2$, 1.2; $MgCl_2$, 1.2; $NaHCO_3$, 25; NaH_2PO_4, 1.25; glucose, 25. All animal experiments were approved by the Tel Aviv University committee on animal care.

Confocal Imaging

Hippocampal neurons were imaged using a FV1000 spectral Olympus confocal microscope using a 60 × 1.2 numerical aperture (NA) water-immersion objective. The experiments were conducted at room temperature in extracellular Tyrode solution containing (in mM) NaCl, 145; KCl, 3; glucose, 15; HEPES, 10; $MgCl_2$, 1.2; $CaCl_2$, 1.2 (pH adjusted to 7.4 with NaOH). To isolate miniature synaptic activity, TTX (0.5 μM) was added to the extracellular solution when indicated.

FRET Imaging and Analysis

Intensity-based FRET imaging was carried as described before (Laviv et al., 2010). Donor dequenching due to the desensitized acceptor was measured from Cer emission (460–500 nm) before and after the acceptor photobleaching. Mean FRET efficiency, E_m, was then calculated using the equation $E_m = 1 - I_{DA}/I_D$, where I_{DA} is the peak of donor emission in the presence of the acceptor and I_D is the peak after acceptor photobleaching (see Supplemental Experimental Procedures for details).

2pFLIM Imaging and Analysis

For imaging in primary cultures, hippocampal neurons were transfected with mEGFP-tagged APP (APP^{mEGFP}) only or APP^{mEGFP} together with APP tagged with mCherry ($APP^{mCherry}$) and visualized 24–36 hr later in Tyrode solution. Fluorescence lifetime images were acquired with a two-photon microscope (LSM 7 MP, Zeiss) coupled to the Becker and Hickl (BH) simple-Tau-152 system. Chameleon Ti:Sapphire laser system with a 80 MHz repetition rate was used to excite the sample. Images were acquired through a Zeiss 63 × 1 NA water-immersion objective for primary cultures and through a Zeiss 20 × 1 NA water-immersion objective for the acute brain slices. A Zeiss dichroic mirror (T690) was used to separate the excitation and the emission light. An additional barrier filter was used to block emission light above 690 nm. Images of 512 × 512 pixels were acquired at a scanning speed of 1.27 μs per pixel. Emission light was separated by a dichroic mirror (555 nm), and the two fluorescent lights were filtered by two band-pass filters (500–550 nm for mEGFP and 590–650 nm for mCherry) placed in front of two hybrid GaAsP detectors (HPM-100-40, BH). The excitation wavelength was 920 nm for the donor fluorophore mEGFP and 1,020 nm for the acceptor fluorophore mCherry. The image acquisition time was 100–120 s to collect a sufficient number of photons. Images were analyzed using the SPCImage software (BH). Regions of interest were marked at boutons. The instrument response function was determined manually and was convoluted with the exponential decay. The lifetime of the donor fluorophore (mEGFP) was then fitted using a monoexponential decay model when APP^{mEGFP} was expressed alone and biexponential one when APP^{mEGFP} was coexpressed with $APP^{mCherry}$. Monoexponential fit ($F(t) = F_0.\exp^{(-t/\tau D)}$) determines the time constant for APP^{mEGFP} lifetime at boutons, τ_D. F_0 is the initial photon counts. Biexponential decay model is composed of a FRET (fast) and a non-FRET (slow) components: $F(t) = F_0.[a_1.\exp^{(-t/\tau AD)} + (100 - a_1)\exp^{(-t/\tau D)}$. In the case of a biexponential fit, τ_m was calculated as $\tau_m = a_1.\tau_{AD} + (100 - a_1).\tau_D$.

FM-Based Imaging and Analysis

Activity-dependent FM1-43 and FM4-64 styryl dyes have been used to estimate basal synaptic vesicle recycling and exocytosis. Action potentials have been elicited by passing 50 mA constant current for 1 ms through two platinum wires, separated by ~7 mm and close to the surface of the coverslip. The extracellular medium contained nonselective antagonist of ionotropic glutamate receptors (kynurenic acid, 0.5 mM) to block recurrent neuronal activity. Synaptic vesicles were loaded with 15 μM FM4-64 or 10 μM FM1-43. FM loading and unloading were done using protocols described previously (Abramov et al., 2009). The fluorescence of individual synapses was determined from the difference between images obtained after staining and after destining (ΔF). To estimate vesicle recycling/release during low-frequency stimulation, we quantified (1) the ΔF signal for staining by 30 action potentials at a rate of 0.2 Hz stimulation (Figure S1A) and (2) the FM destaining rate during 1 Hz stimulation following staining of boutons by maximal stimulation (Figure S1C). Detection of signals has been done using custom-written scripts in MATLAB (Mathworks) as described before (Abramov et al., 2009).

Statistical Analysis

Error bars shown in the figures represent SEM. The number of boutons is defined by *n* and the number of experiments (cultures) by *N*. All the experiments were repeated at least in three different batches of cultures. One-way ANOVA analysis with post hoc Dunnett or Bonferroni correction was used to compare several conditions. Student's unpaired t test was used in the experiments where two populations of synapses were compared. Student's paired t test was used when the same population of synapses was tested before and after treatment. *$p < 0.05$; **$p < 0.01$; ***$p < 0.001$; ns, not significant.

Additional experimental procedures can be found in the Supplemental Experimental Procedures.

SUPPLEMENTAL INFORMATION

Supplemental Information includes Supplemental Experimental Procedures and eight figures and can be found with this article online at http://dx.doi.org/10.1016/j.celrep.2014.04.024.

AUTHOR CONTRIBUTIONS

H.F. designed, performed, and analyzed the experiments presented in Figures 1, 2, 3A–3D, 5B, 6, 7, and 8 and Figures S1, S3–S5, and S7 with the help of N.G. and E.S. S.F. established the 2pFLIM system and designed, performed, and analyzed the 2pFLIM-FRET experiments (Figures 3E–3J and 8). I. Shapira and Y.B. generated the constructs. I. Shapira generated lentiviruses for in vivo injection. O.S. and J.A.H. contributed biochemical data presented in Figures 5A, S2, and S6. S.B. and E.Y.I. contributed single-molecule subunit counting experiments presented in Figure 4. T.O. and D.M.W. provided Aβ40S26C dimers and advised on biochemistry. H.F., S.F., and I. Slutsky wrote the manuscript. I. Slutsky conceived and supervised the project.

ACKNOWLEDGMENTS

We thank Dr. Gerd Multhaup for the comments on the manuscript, Dr. Avraham Yaron for advice on the Aβ40-biotin binding assay, Dr. Ruth Gabizon for providing PrP^C knockout mice, and all the lab members for help and discussions. This work was supported by a European Research Council starting grant (281403, I. Slutsky), the Legacy Heritage Biomedical Program of the Israel Science Foundation (865/11, to I. Slutsky), the Alzheimer's Association (NIRG-10-172308, to I. Slutsky), the Israel Science Foundation (993/08, 170/08, and 398/13, to I. Slutsky), Marie Curie CIG grant 33458 (to S.F.), the Foundation for Neurologic Diseases (DMW), NIH grant R01 NS35549 (to E.Y.I.), and by a Deutsche Israel Programme grant (to J.A.H.). I. Slutsky is grateful to Sheila and Denis Cohen Charitable Trust and Rosetrees Trust of the UK for their support. S.F. is grateful to the Center for Nanoscience and Nanotechnology of Tel Aviv University for the award of postdoctoral fellowship.

Received: August 28, 2012
Revised: March 12, 2014
Accepted: April 12, 2014
Published: May 15, 2014

REFERENCES

Abramov, E., Dolev, I., Fogel, H., Ciccotosto, G.D., Ruff, E., and Slutsky, I. (2009). Amyloid-beta as a positive endogenous regulator of release probability at hippocampal synapses. Nat. Neurosci. *12*, 1567–1576.

Acsády, L., Kamondi, A., Sík, A., Freund, T., and Buzsáki, G. (1998). GABAergic cells are the major postsynaptic targets of mossy fibers in the rat hippocampus. J. Neurosci. *18*, 3386–3403.

Bacskai, B.J., Skoch, J., Hickey, G.A., Allen, R., and Hyman, B.T. (2003). Fluorescence resonance energy transfer determinations using multiphoton fluorescence lifetime imaging microscopy to characterize amyloid-beta plaques. J. Biomed. Opt. *8*, 368–375.

Bai, Y., Markham, K., Chen, F., Weerasekera, R., Watts, J., Horne, P., Wakutani, Y., Bagshaw, R., Mathews, P.M., Fraser, P.E., et al. (2008). The in vivo brain interactome of the amyloid precursor protein. Mol. Cell. Proteomics *7*, 15–34.

Bakker, A., Krauss, G.L., Albert, M.S., Speck, C.L., Jones, L.R., Stark, C.E., Yassa, M.A., Bassett, S.S., Shelton, A.L., and Gallagher, M. (2012). Reduction of hippocampal hyperactivity improves cognition in amnestic mild cognitive impairment. Neuron *74*, 467–474.

Benilova, I., Karran, E., and De Strooper, B. (2012). The toxic Aβ oligomer and Alzheimer's disease: an emperor in need of clothes. Nat. Neurosci. *15*, 349–357.

Buckner, R.L., Snyder, A.Z., Shannon, B.J., LaRossa, G., Sachs, R., Fotenos, A.F., Sheline, Y.I., Klunk, W.E., Mathis, C.A., Morris, J.C., and Mintun, M.A. (2005). Molecular, structural, and functional characterization of Alzheimer's disease: evidence for a relationship between default activity, amyloid, and memory. J. Neurosci. *25*, 7709–7717.

Busche, M.A., Eichhoff, G., Adelsberger, H., Abramowski, D., Wiederhold, K.H., Haass, C., Staufenbiel, M., Konnerth, A., and Garaschuk, O. (2008). Clusters of hyperactive neurons near amyloid plaques in a mouse model of-Alzheimer's disease. Science *321*, 1686–1689.

Busche, M.A., Chen, X., Henning, H.A., Reichwald, J., Staufenbiel, M., Sakmann, B., and Konnerth, A. (2012). Critical role of soluble amyloid-β for early hippocampal hyperactivity in a mouse model of Alzheimer's disease. Proc. Natl. Acad. Sci. USA *109*, 8740–8745.

Cirrito, J.R., Yamada, K.A., Finn, M.B., Sloviter, R.S., Bales, K.R., May, P.C., Schoepp, D.D., Paul, S.M., Mennerick, S., and Holtzman, D.M. (2005). Synaptic activity regulates interstitial fluid amyloid-beta levels in vivo. Neuron *48*, 913–922.

Citron, M., Teplow, D.B., and Selkoe, D.J. (1995). Generation of amyloid beta protein from its precursor is sequence specific. Neuron *14*, 661–670.

Dahms, S.O., Hoefgen, S., Roeser, D., Schlott, B., Gührs, K.H., and Than, M.E. (2010). Structure and biochemical analysis of the heparin-induced E1 dimer of the amyloid precursor protein. Proc. Natl. Acad. Sci. USA *107*, 5381–5386.

Dolev, I., Fogel, H., Milshtein, H., Berdichevsky, Y., Lipstein, N., Brose, N., Gazit, N., and Slutsky, I. (2013). Spike bursts increase amyloid-β 40/42 ratio by inducing a presenilin-1 conformational change. Nat. Neurosci. *16*, 587–595.

Eggert, S., Midthune, B., Cottrell, B., and Koo, E.H. (2009). Induced dimerization of the amyloid precursor protein leads to decreased amyloid-beta protein production. J. Biol. Chem. *284*, 28943–28952.

Hsia, A.Y., Masliah, E., McConlogue, L., Yu, G.Q., Tatsuno, G., Hu, K., Kholodenko, D., Malenka, R.C., Nicoll, R.A., and Mucke, L. (1999). Plaque-independent disruption of neural circuits in Alzheimer's disease mouse models. Proc. Natl. Acad. Sci. USA *96*, 3228–3233.

Jankowsky, J.L., Fadale, D.J., Anderson, J., Xu, G.M., Gonzales, V., Jenkins, N.A., Copeland, N.G., Lee, M.K., Younkin, L.H., Wagner, S.L., et al. (2004). Mutant presenilins specifically elevate the levels of the 42 residue beta-amyloid peptide in vivo: evidence for augmentation of a 42-specific gamma secretase. Hum. Mol. Genet. *13*, 159–170.

Kaden, D., Voigt, P., Munter, L.-M., Bobowski, K.D., Schaefer, M., and Multhaup, G. (2009). Subcellular localization and dimerization of APLP1 are strikingly different from APP and APLP2. J. Cell Sci. *122*, 368–377.

Kamenetz, F., Tomita, T., Hsieh, H., Seabrook, G., Borchelt, D., Iwatsubo, T., Sisodia, S., and Malinow, R. (2003). APP processing and synaptic function. Neuron *37*, 925–937.

Kang, J., Lemaire, H.G., Unterbeck, A., Salbaum, J.M., Masters, C.L., Grzeschik, K.H., Multhaup, G., Beyreuther, K., and Müller-Hill, B. (1987). The precursor of Alzheimer's disease amyloid A4 protein resembles a cell-surface receptor. Nature *325*, 733–736.

Koo, E.H., and Squazzo, S.L. (1994). Evidence that production and release of amyloid beta-protein involves the endocytic pathway. J. Biol. Chem. *269*, 17386–17389.

Laviv, T., Riven, I., Dolev, I., Vertkin, I., Balana, B., Slesinger, P.A., and Slutsky, I. (2010). Basal GABA regulates GABA(B)R conformation and release probability at single hippocampal synapses. Neuron *67*, 253–267.

Laviv, T., Vertkin, I., Berdichevsky, Y., Fogel, H., Riven, I., Bettler, B., Slesinger, P.A., and Slutsky, I. (2011). Compartmentalization of the GABAB receptor signaling complex is required for presynaptic inhibition at hippocampal synapses. J. Neurosci. *31*, 12523–12532.

Lorenzo, A., Yuan, M., Zhang, Z., Paganetti, P.A., Sturchler-Pierrat, C., Staufenbiel, M., Mautino, J., Vigo, F.S., Sommer, B., and Yankner, B.A. (2000). Amyloid beta interacts with the amyloid precursor protein: a potential toxic mechanism in Alzheimer's disease. Nat. Neurosci. *3*, 460–464.

Marcello, E., Gardoni, F., Mauceri, D., Romorini, S., Jeromin, A., Epis, R., Borroni, B., Cattabeni, F., Sala, C., Padovani, A., and Di Luca, M. (2007). Synapse-associated protein-97 mediates α-secretase ADAM10 trafficking and promotes its activity. J. Neurosci. *27*, 1682–1691.

Melchor, J.P., and Van Nostrand, W.E. (2000). Fibrillar amyloid beta-protein mediates the pathologic accumulation of its secreted precursor in human cerebrovascular smooth muscle cells. J. Biol. Chem. *275*, 9782–9791.

Mucke, L., and Selkoe, D.J. (2012). Neurotoxicity of amyloid β protein: synaptic and network dysfunction. Cold Spring Harb. Perspect. Med. *2*, a006338.

Munter, L.M., Voigt, P., Harmeier, A., Kaden, D., Gottschalk, K.E., Weise, C., Pipkorn, R., Schaefer, M., Langosch, D., and Multhaup, G. (2007). GxxxG motifs within the amyloid precursor protein transmembrane sequence are critical for the etiology of Abeta42. EMBO J. *26*, 1702–1712.

Nishimoto, I., Okamoto, T., Matsuura, Y., Takahashi, S., Okamoto, T., Murayama, Y., and Ogata, E. (1993). Alzheimer amyloid protein precursor complexes with brain GTP-binding protein G(o). Nature *362*, 75–79.

O'Nuallain, B., Freir, D.B., Nicoll, A.J., Risse, E., Ferguson, N., Herron, C.E., Collinge, J., and Walsh, D.M. (2010). Amyloid beta-protein dimers rapidly form stable synaptotoxic protofibrils. J. Neurosci. *30*, 14411–14419.

Okamoto, T., Takeda, S., Murayama, Y., Ogata, E., and Nishimoto, I. (1995). Ligand-dependent G protein coupling function of amyloid transmembrane precursor. J. Biol. Chem. *270*, 4205–4208.

Palop, J.J., and Mucke, L. (2010). Amyloid-beta-induced neuronal dysfunction in Alzheimer's disease: from synapses toward neural networks. Nat. Neurosci. *13*, 812–818.

Palop, J.J., Chin, J., Roberson, E.D., Wang, J., Thwin, M.T., Bien-Ly, N., Yoo, J., Ho, K.O., Yu, G.Q., Kreitzer, A., et al. (2007). Aberrant excitatory neuronal activity and compensatory remodeling of inhibitory hippocampal circuits in mouse models of Alzheimer's disease. Neuron *55*, 697–711.

Perez, R.G., Soriano, S., Hayes, J.D., Ostaszewski, B., Xia, W., Selkoe, D.J., Chen, X., Stokin, G.B., and Koo, E.H. (1999). Mutagenesis identifies new signals for β-amyloid precursor protein endocytosis, turnover, and the generation of secreted fragments, including Abeta42. J. Biol. Chem. *274*, 18851–18856.

Rossjohn, J., Cappai, R., Feil, S.C., Henry, A., McKinstry, W.J., Galatis, D., Hesse, L., Multhaup, G., Beyreuther, K., Masters, C.L., and Parker, M.W. (1999). Crystal structure of the N-terminal, growth factor-like domain of Alzheimer amyloid precursor protein. Nat. Struct. Biol. *6*, 327–331.

Scheuermann, S., Hambsch, B., Hesse, L., Stumm, J., Schmidt, C., Beher, D., Bayer, T.A., Beyreuther, K., and Multhaup, G. (2001). Homodimerization of amyloid precursor protein and its implication in the amyloidogenic pathway of Alzheimer's disease. J. Biol. Chem. *276*, 33923–33929.

Shaked, G.M., Kummer, M.P., Lu, D.C., Galvan, V., Bredesen, D.E., and Koo, E.H. (2006). Abeta induces cell death by direct interaction with its cognate extracellular domain on APP (APP 597-624). FASEB J. *20*, 1254–1256.

Shaked, G.M., Chauv, S., Ubhi, K., Hansen, L.A., and Masliah, E. (2009). Interactions between the amyloid precursor protein C-terminal domain and G proteins mediate calcium dysregulation and amyloid beta toxicity in Alzheimer's disease. FEBS J. *276*, 2736–2751.

Shankar, G.M., Li, S., Mehta, T.H., Garcia-Munoz, A., Shepardson, N.E., Smith, I., Brett, F.M., Farrell, M.A., Rowan, M.J., Lemere, C.A., et al. (2008). Amyloid-beta protein dimers isolated directly from Alzheimer's brains impair synaptic plasticity and memory. Nat. Med. *14*, 837–842.

Swanson, T.L., Knittel, L.M., Coate, T.M., Farley, S.M., Snyder, M.A., and Copenhaver, P.F. (2005). The insect homologue of the amyloid precursor protein interacts with the heterotrimeric G protein Go α in an identified population of migratory neurons. Dev. Biol. *288*, 160–178.

Townsend, M., Shankar, G.M., Mehta, T., Walsh, D.M., and Selkoe, D.J. (2006). Effects of secreted oligomers of amyloid beta-protein on hippocampal synaptic plasticity: a potent role for trimers. J. Physiol. *572*, 477–492.

Ulbrich, M.H., and Isacoff, E.Y. (2007). Subunit counting in membrane-bound proteins. Nat. Methods *4*, 319–321.

Van Nostrand, W.E., Melchor, J.P., Keane, D.M., Saporito-Irwin, S.M., Romanov, G., Davis, J., and Xu, F. (2002). Localization of a fibrillar amyloid beta-protein binding domain on its precursor. J. Biol. Chem. *277*, 36392–36398.

Verret, L., Mann, E.O., Hang, G.B., Barth, A.M.I., Cobos, I., Ho, K., Devidze, N., Masliah, E., Kreitzer, A.C., Mody, I., et al. (2012). Inhibitory interneuron deficit links altered network activity and cognitive dysfunction in Alzheimer model. Cell *149*, 708–721.

Vossel, K.A., Beagle, A.J., Rabinovici, G.D., Shu, H., Lee, S.E., Naasan, G., Hegde, M., Cornes, S.B., Henry, M.L., Nelson, A.B., et al. (2013). Seizures and epileptiform activity in the early stages of Alzheimer disease. JAMA Neurol. *70*, 1158–1166.

Walsh, D.M., Klyubin, I., Fadeeva, J.V., Cullen, W.K., Anwyl, R., Wolfe, M.S., Rowan, M.J., and Selkoe, D.J. (2002). Naturally secreted oligomers of amyloid beta protein potently inhibit hippocampal long-term potentiation in vivo. Nature *416*, 535–539.

Yasuda, R., Harvey, C.D., Zhong, H., Sobczyk, A., van Aelst, L., and Svoboda, K. (2006). Supersensitive Ras activation in dendrites and spines revealed by two-photon fluorescence lifetime imaging. Nat. Neurosci. *9*, 283–291.

Zheng, H., Jiang, M., Trumbauer, M.E., Sirinathsinghji, D.J., Hopkins, R., Smith, D.W., Heavens, R.P., Dawson, G.R., Boyce, S., Conner, M.W., et al. (1995). beta-Amyloid precursor protein-deficient mice show reactive gliosis and decreased locomotor activity. Cell *81*, 525–531.